Ocean Engineering 268 (2023) 113161

Contents lists available at ScienceDirect

Ocean Engineering

journal homepage: www.elsevier.com/locate/oceaneng

Directional wave measurements from navigational buoys ☆

Camilla Saetre [a,c,*], Harald Tholo [b], Jostein Hovdenes [b], Jan Kocbach [c], Anne Ansnes Hageberg [c], Inge Klepsvik [c], Ole Johan Aarnes [d], Birgitte Rugaard Furevik [d,e], Anne Karin Magnusson [d]

[a] University of Bergen, Department of Physics and Technology, UiB, Allègaten 55, Bergen, N-5007, Norway
[b] Aanderaa Data Instruments AS, Sanddalsringen 5b, Bergen, N-5225 Nesttun, Norway
[c] NORCE Norwegian Research Centre AS, P.O.B 22 Nygårdstangen, Bergen, N-5838, Norway
[d] The Norwegian Meteorological Institute, Allègaten 70, Bergen, N-5007, Norway
[e] University of Bergen, Bergen Offshore Wind Centre, Geophysical Institute, UiB, Allègaten 55, Bergen, N-5007, Norway

ARTICLE INFO

Keywords:
Wave measurement
Buoy
Navigational buoy
Inter-comparison
MOTUS

ABSTRACT

In-situ wave measurements are often required by marine industry standards and for verification of coastal wave forecasts. Obtaining wave measurements is costly and it would be advantageous to utilize existing platforms like navigational buoys designed for environmental monitoring. In this study, a wave sensor module (MOTUS Wave Sensor, Aanderaa Data Instruments) installed on a navigational buoy (Tideland) and a coastal buoy (EMM2.0) is validated against a dedicated wave measurement buoy (Waverider, Datawell). The validation is based upon four months of measurements off the west coast of Norway. The results show that the MOTUS sensor on-board navigational/coastal buoys provide accurate measurements of wave parameters compared to Waverider. Wave height biases were less than 0.04 m over the full wave spectra, and less than 5% for frequencies between 0.05 and 0.45 Hz (0.01 Hz bin width). Mean wave direction bias for the full spectra was 1.4 and 2.8 degrees, and less than 5 and 10 degrees in frequency bins between 0.05 and 0.45 Hz for the navigational and coastal buoy, respectively. External compass measurements were required for accurate directional measurements for the coastal buoy. The validated wave sensor provides in-situ directional wave measurements with measurement uncertainties well within recommended accuracy levels.

1. Introduction

Norway's coastline is 103,000 km, including all islands, islets and fjords, the second longest coastline in the world. Obtaining wave height and wave direction measurements in strategic areas is required to validate and improve numerical modelling and forecasting of ocean waves (e.g. yr.no and barentswatch.no). Open-access 2 Hz wave measurements carried out by the Norwegian Public Roads Administration in Sulafjord (2016–2020) (Furevik et al., 2020, 2016) have shed new light on wave modelling in narrow fetch geometry (Christakos et al., 2021, 2020). Also, for other metocean parameters (wind, temperature, and currents) buoys may provide unique data for validation of numerical models (Cavaleri et al., 2018). Wind measurements carried out on land are often sheltered and do not represent the fjord or open ocean conditions well and oceanographic measurements are sparse. Coastal in situ measurements of wave height and direction, distributed in near real-time, are therefore highly valued both by the commercial and leisure fleet.

Wave buoys are in many respects considered to be a highly reliable source of offshore and coastal wave data and are often considered a benchmark. They are extensively used in wave forecasting, particularly for validation and calibration of numerical models and satellite altimetry, respectively. They provide standalone data sets often utilized for a range of wave related research. The principle of a wave buoy is a floating device following the surface and recording the time series of the buoy's movement in all three directions. Statistics of the wave field can be calculated from a time series or a spectrum. The first wave buoy from Datawell, the Datawell Waverider which was launched in 1968 was dedicated to wave height measurements, while the Datawell Wavec launched in 1983 and later versions of the Datawell Waverider were dedicated to wave height and direction measurements. The Waverider is recommended as a relative reference at deep and intermediate water

☆ This work was part of the research project Flexible and cost-effective wave sensor, coordinated by Aanderaa Data Instruments AS, funded by the Research Council of Norway (project no. 256521).

* Corresponding author at: University of Bergen, Department of Physics and Technology, UiB, Allègaten 55, Bergen, N-5007, Norway.
E-mail address: camilla.satre@uib.no (C. Saetre).
URL: https://www.uib.no/en/persons/Camilla.S%C3%A6tre (C. Saetre).

https://doi.org/10.1016/j.oceaneng.2022.113161
Received 4 May 2022; Received in revised form 9 September 2022; Accepted 12 November 2022
Available online 9 December 2022

wave evaluations (Jensen et al., 2011; Luther et al., 2013). Longuet-Higgins et al. (1965) described the calculations of the directional wave spectra from floating buoy movements.

Setting up a network of dedicated wave buoys like the Datawell Waverider or large metocean buoys that combine wave buoys with other meteorological or oceanographic measurements is costly; such buoys suffer from limited battery lifetime, bio-fouling, and requirement for data transfer, which make them costly to install and maintain. An attractive alternative would be to equip the existing network of navigational and coastal buoys with low-cost wave measurement sensors. Coastal buoys are used to monitor environmental parameters in coastal regions, whereas navigational buoys are primarily markers for ships and boat traffic. The Norwegian Coastal Administration (NCA) carries the national responsibility in Norway for safety at sea and develops and maintains fairways along the coast marked with lighthouses, land-based markings, and navigational buoys. The buoys are regularly serviced, addressing issues of battery lifetime, bio-fouling and data transfer, and could be utilized as sensor platforms for wind, wave and current measurements, i.e. smart buoys. They could even be equipped with Automatic Identification System (AIS) and broadcast the metocean recordings to passing ships. Marker buoys in connection to aqua farms could be another platform. Globally, there are a large number of deployed navigational buoys, some of which may be suited for wave measurements. In Norway there are approximately 20 navigational buoys in potentially useful locations.

It has been considered challenging to achieve acceptable accuracy for wave parameters when equipping navigational or coastal buoys with wave sensors, especially for parameters related to wave direction (Jensen et al., 2021). Wave measurements are closely integrated with the buoy properties as well as the properties of the mooring; a navigational buoy is moored to stay on location, and the shape and weight are not optimized for wave measurements. Equipping such buoys with low-cost wave sensors, the question is what accuracy can be achieved compared to a dedicated wave buoy. The accuracy for heave measurements from Waverider is 0.5% after calibration (less than 1% after 3 years), and the directional resolution is 1.4 degrees with heading error up to 2 degrees (Datawell BV, 2020). For heave measurements, satellite observations are an alternative to in situ measurements. Comparisons of wave height of model, in situ and satellite observations (Jason-2 SAR Mode) show deviations less than 5%, and correlation above 0.95 (Abdalla et al., 2018). Cavaleri et al. (2018) stress the importance of evaluation of measurement accuracy when comparing and validating wave models to in situ or remote measurements.

Previous studies have addressed wave measurement inter-comparison (Krogstad et al., 1999; Liu et al., 2015; Cavaleri et al., 2018; Jensen et al., 2021), where various means of inter-comparing wave parameters and spectra are discussed. Wave measurement inter-comparison is a complex task as comparisons need to be done for a wide range of wave heights and wave frequencies, including frequency dependent directional components (Jensen et al., 2011). Also, finite depth mechanisms such as shoaling and refraction affect the measurements and are frequency dependent, affecting the energy and directional attributes (Cavaleri et al., 2018). Additionally, when validating a sensor, it may be a challenge that the data are often collected from different kinds of instruments, leading to the use of different sampling strategies and different analysis procedures (Krogstad et al., 1999). One structured approach for wave measurement inter-comparison is to compare wave height and directional parameters based on Fourier coefficients at distinct frequency and energy bins of the entire wave spectrum. This approach is e.g. applied in the WavEval Tool developed in the Coastal Data Information Program (CDIP) (Jensen et al., 2011; Luther et al., 2013; Cavaleri et al., 2018; Alliance for Coastal Technologies, 2007).

Buoy-based wave sensors can utilize either a Global Navigation Satellite System (GNSS) sensor, or a solution involving a 3D accelerometer to calculate the vertical and horizontal displacement. GNSS-based technologies require more power, and there is a risk of losing the GPS-signal at higher sea states (Herbers et al., 2012), thus accelerometer-based technologies are preferable for continuous long-term measurements. Accelerometer-based wave sensors can be divided into two different subgroups. Either, the accelerometer must be kept horizontal by means of a gyroscope, or the calculations must make use of the orientation of the accelerometer. The Waverider is of the first type, while the MOTUS wave sensor (Aanderaa Data Instruments, Bergen, Norway) is of the second type. The paper of Liu et al. (2020) and references therein describes these two methods of wave observation by accelerometers.

Fig. 1. MOTUS Wave Sensor. Dimensions 130 × 130 × 110 mm and weight of 1.23 kg.

The objective of this study is to investigate the quality of wave measurements carried out in 2017–2018 with the Aanderaa Data Instruments AS (AADI) MOTUS wave sensor, mounted on a Tideland SB-138P Sentinel©buoy (Tideland, a Xylem brand, 2022) and an YSI EMM2.0 Coastal buoy (Xylem Analytics, 2022), (hereafter denoted Tideland and EMM). Tideland is a common navigational buoy, whereas EMM is a sensor platform buoy which can also be utilized as a marking buoy. In this paper both buoys are referred to as navigational buoys. The survey was carried out as part of the development of the MOTUS motion sensors by AADI. Tengberg et al. (2018) presented initial comparisons from this survey.

The outline of the paper is as follows; the experimental setup, validation method and overall conditions during the experiment are described in Section 2. The results of the validations are presented in Section 3, for wave height and direction. Discussion and conclusions are given in Sections 4 and 5.

2. Experimental setup and method

2.1. Directional wave sensors used in the experiment

Fig. 1 shows a picture of the MOTUS sensor, key information and pictures of the three buoys are included in Fig. 2. The MOTUS wave sensor has a depth rating of 30 m, operating temperature of −40 to +70 °C, dimensions of 130 × 130 × 110 mm and weight of 1.23 kg, including bracket. Three different buoys were included in the inter-comparison; a Datawell Waverider MKIII buoy (used as reference), a Tideland SB138P navigational buoy with the AADI MOTUS wave sensor mounted approximately 30 cm off centre, and an EMM2.0 Coastal buoy (sensor platform buoy) with two installed AADI MOTUS wave sensors: one installed near the rotational centre of the buoy, and the other close to the edge of the upper deck. Both sensors on EMM are used in the analysis. EMM comparisons for December 2017–March 2018 from the centre mounted sensor, and March 2018 also from the off-centre sensor.

According to the Waverider MKIII manual (Datawell BV, 2020), the Waverider sensor is placed in a gyroscope whose motion is damped

Fig. 2. Left: Waverider Datawell BV (Diameter 70 cm, Datawell BV, 2020) Centre: Tideland SB138P navigation buoy (diameter 175 cm, height 229 cm). Right: EMM2.0 Coastal monitoring buoy (diameter 200 cm, height 328 cm).

with oil, and is based on a micro-electro-mechanical system (MEMS) 3-axis accelerometer. For the buoy orientation and the wave direction, a 3-axis Flux gate compass is used. By using a stabilized accelerometer platform there will be no need for pitch and roll rotation of the accelerometer output. The accelerometer signal is low pass filtered and double integrated in the frequency domain. The Waverider provides parameters based on both frequency domain as well as time domain.

The MOTUS wave sensor is based on an Attitude Heading Reference System (AHRS) that consists of a 3-axis gyroscope, a 3-axis magnetometer, and a 3-axis accelerometer. In the MOTUS, the oil filled self-stabilized accelerometer and the Flux gate compass used in Waverider have been replaced by a single MEMS chip. By utilizing data fusion between the three datasets delivered in the MEMS chip, the orientation of the sensor platform is calculated at an output rate of 100 Hz. The sensor orientation is used to convert the sensor referred 3-axis acceleration into Earth referred (ENU) acceleration. The acceleration signal is band pass filtered to match the wave bandwidth of interest. To convert the 3-axis acceleration into 3-axis displacement, a double integration is performed in the frequency domain by means of Fast Fourier Transform (FFT). The sensor can be set up to use record lengths from 5 min to 60 min for calculation of wave data, such as integrated wave parameters and wave spectra. Record lengths of 30 min are used in this study. The MOTUS sensor provides wave parameters based on both frequency domain and time domain calculations. In time domain mode, simultaneous measurements of ocean currents by an in-line Doppler Current Sensor (DCS) are also available. The DCS measurements are used qualitatively in this study to identify periods with strong ocean currents.

2.2. Location and conditions

The two navigational buoys and the Waverider were deployed at a test area about 18 km west of Karmøy, Norway in 2017 and 2018 (Fig. 3). The first part of the deployment was used for algorithm development, and the last part was used for validation with unchanged measurement setup for the buoys and sensors (December 2017 to March 2018). Fig. 4 shows an overview of the deployment period.

The buoy moorings consisted of combinations of floaters and sinkers as shown in Fig. 5. For the EMM buoy, the last cord close to the chain below the buoy was a rubber cord that allows for the buoy to move

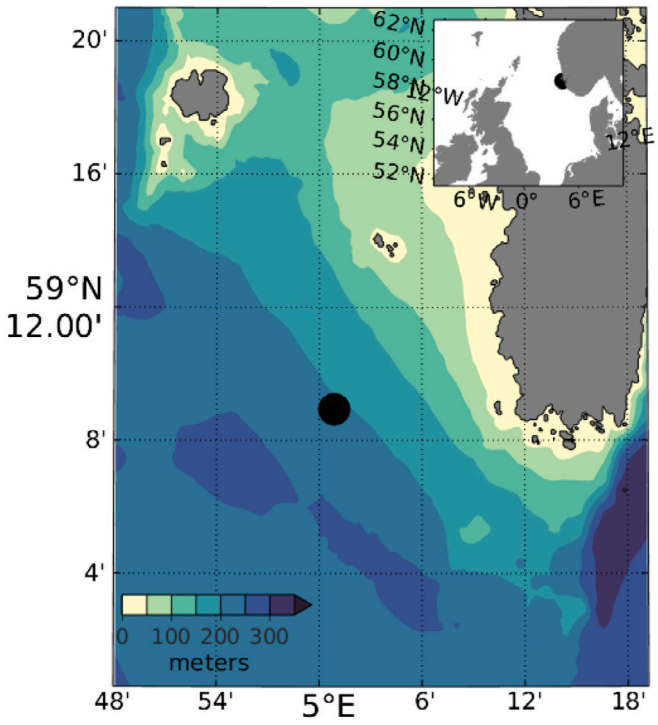

Fig. 3. Location of the buoys west of Karmøy, Norway, marked with a black circle; 59.39° N, 5.25° E. Colour scaled isobaths with depth in metre, depth at buoy location was 200 m. (For interpretation of the references to colour in this figure legend, the reader is referred to the web version of this article.)

more flexibly. For the Tideland buoy, a polyester rope was used for the last cord in the validation period. Both systems used a concrete block as anchor weight. The impact of the mooring is expected to vary with the ocean current, where a strong current will cause an increased drag force along the mooring line and reduce the buoy's ability to move freely.

The water depth at the buoy location site is approximately 200 m. The design of the mooring will always be a compromise between horizontal drift, the ability for the buoy/mooring system to withstand

	2017											2018			
	F	M	A	M	J	J	A	S	O	N	D	J	F	M	A
Algorithm development period															
Wave height and direction comparison period															
Evaluation of external compass period															

Fig. 4. Breakdown of deployment period.

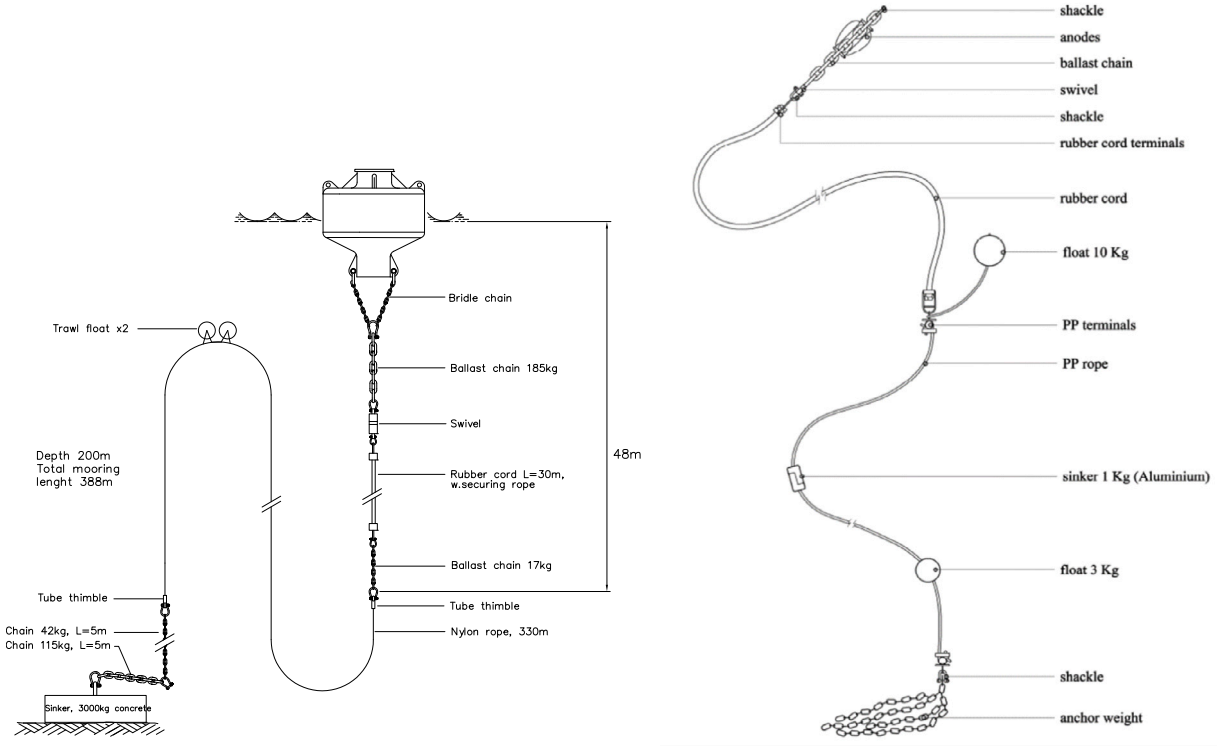

Fig. 5. (a) Mooring of Tideland SP138/EMM 2.0 buoy. (b) Mooring of Datawell waverider MKIII, 0.7 m buoy.
Source: Figure taken from Datawell BV (2020).

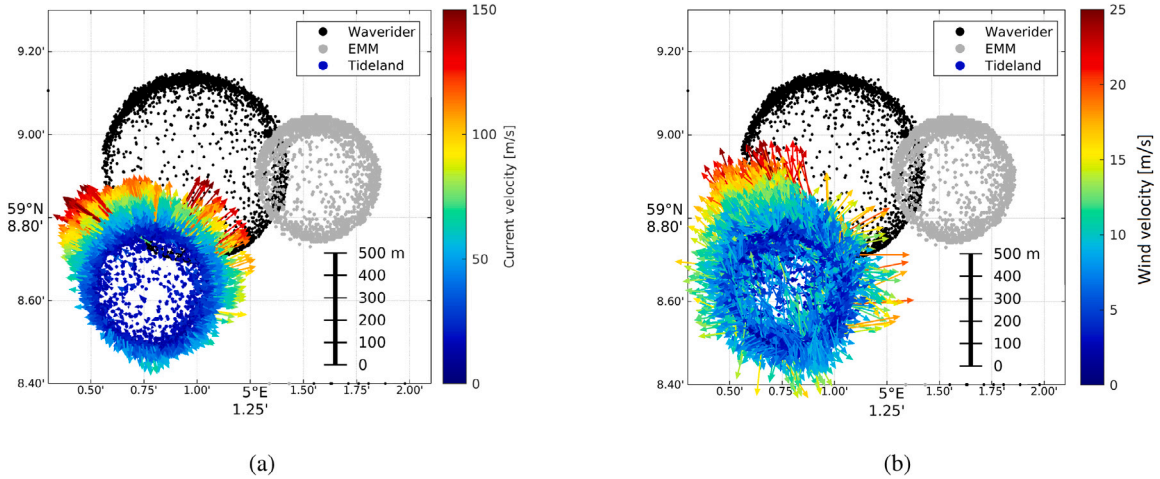

Fig. 6. Buoy positioning over the period January–March 2018; Waverider (black dots) and the two navigational buoys Tideland (blue dots, with vectors) and EMM (grey dots). (a) Current vectors and (b) wind vectors are added on actual positions of the Tideland buoy. (For interpretation of the references to colour in this figure legend, the reader is referred to the web version of this article.)

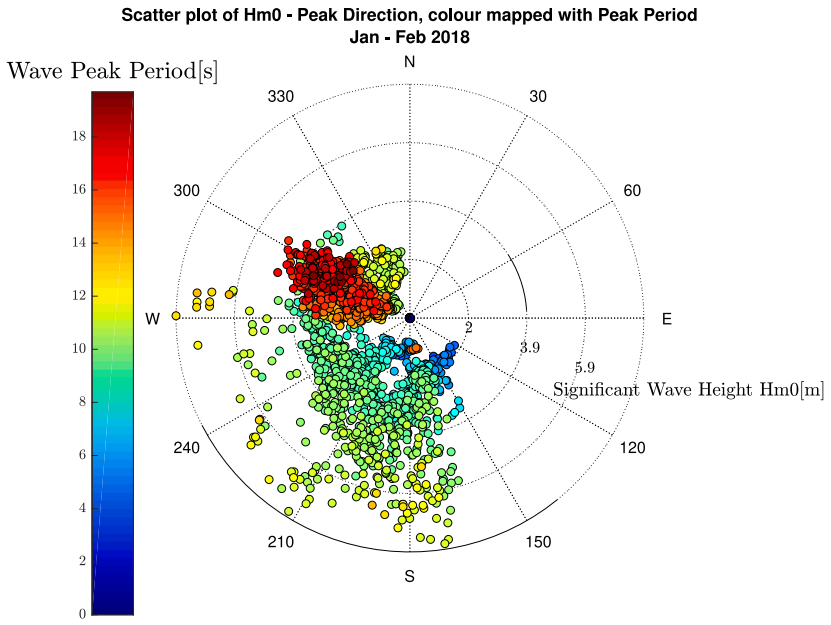

Fig. 7. Wave peak direction (coming from) vs H_{m0} and peak period, January–February 2018 (colour scale 0–19 s). (For interpretation of the references to colour in this figure legend, the reader is referred to the web version of this article.)

strong currents, and to be sufficiently resilient to not affect the wave measurements itself. The MKIII manual for the Waverider (0.7 m buoy) states that for a current speed of 1.0 m/s, standard mooring lay-out is applicable at a maximum mooring depth of 180 m (Datawell BV, 2020). In stronger current conditions the buoy can be submerged by the mooring tension. At 200 m the applicable current speed will be slightly less. During the trials we experienced such strong currents and corresponding lack of data for short periods of time for the Waverider measurements. We assume the missing data points were caused by the smaller Waverider being pulled under due to the strong currents. Due to the larger buoyancy of the Tideland and the EMM, this was not an issue for these buoys during the deployment.

The test area west of Karmøy is located offshore and with fairly constant depth. Thus the wave conditions are expected to be relatively homogeneous. The currents are mostly going northward (the Norwegian coastal current) but strong eddies occur. These are triggered by the sharp bend in the coastline south of the area and when the Norwegian coastal current meets with a branch of the North Atlantic Current. Fig. 6 shows the variation in buoy position for the three buoys in the period January–March 2018. Currents measured on Tideland are displayed as arrows in Fig. 6(a), and show how the currents move the buoy into the outer positions of the mooring. The Waverider has the longest mooring and thus illustrates the largest circle in the map. The movement of the buoys was limited within a diameter of approximately 500 m for the navigational buoys (Tideland and EMM) and 800 m for the Waverider. The trajectories indicate that the mooring lines were often fully stretched. This was mainly due to the local current conditions and less affected by the local wind, which is illustrated by the corresponding wind vectors obtained with the Tideland-buoy (Fig. 6b). It is seen that the current vectors are consistently pointing in a radial direction relative to the position of the buoy, while the corresponding wind vectors are less organized.

Fig. 7 shows the wave conditions as measured by Waverider from January–February 2018. A rose diagram shows the wave peak direction (arriving from, meteorological convention). The colour scale is for wave peak period, and radial axes give significant wave height, H_{m0}, values (circles every 2 m, from 0 to 8 m). In the period shown, the highest cases were from west and south. The red dots in Fig. 7 indicate presence of very long swell (17–19 s) coming in from northwest.

2.3. Validation method

For comparison of the different wave measurements, we have used the WavEval Tool developed in the Coastal Data Information Program (CDIP) (Jensen et al., 2011; Luther et al., 2013; Cavaleri et al., 2018; Alliance for Coastal Technologies, 2007). This tool compares two datasets of concurrent wave height and directional parameters based on the first five Fourier coefficients (OReilly et al., 1996), at distinct frequency and energy bins of the entire wave spectrum. The measurement frequency resolution is 0.005 Hz for Waverider and 0.004 Hz for MOTUS, and a resolution of 0.01 Hz is used for the combined comparison with logarithmic energy bands between 10^{-4} to 10^{4} m^2.

The wave measurements from MOTUS and Waverider are based on the time series measurements of three-axis acceleration. The heave motion is calculated from the double integral of time series for the vertical acceleration. Fast Fourier transform with Hanning window function is applied to the three-axis acceleration time series, providing acceleration in the frequency domain. The acceleration vectors in the three directions can be written as:

$$\begin{aligned} A_{xf} &= \alpha_{xf} + i\beta_{xf} \\ A_{yf} &= \alpha_{yf} + i\beta_{yf} \\ A_{zf} &= \alpha_{zf} + i\beta_{zf} \end{aligned} \tag{1}$$

Here α and β are Fourier coefficients. Subscripts x, y, and z denote North, West, and vertical directions, respectively, and f indicates the frequency domain. From the acceleration vectors, co-spectra and quadrature spectra can be calculated. For x and y directions the spectra are given as:

$$C_{xy} = \vec{A_{xf}} \cdot \vec{A_{yf}} = \alpha_{xf}\alpha_{yf} + \beta_{xf}\beta_{yf} \tag{2}$$

$$Q_{xy} = \vec{A_{xf}} \times \vec{A_{yf}} = \alpha_{xf}\beta_{yf} - \beta_{xf}\alpha_{yf} \tag{3}$$

There are equivalent equations for the other combinations of directions. The co-spectra and quadrature spectra matrices are given as:

$$\begin{bmatrix} C_{xx} & C_{xy} & C_{xz} \\ C_{yx} & C_{yy} & C_{yz} \\ C_{zx} & C_{zy} & C_{zz} \end{bmatrix} \tag{4}$$

$$\begin{bmatrix} 0 & 0 & Q_{xz} \\ 0 & 0 & Q_{yz} \\ Q_{zx} & Q_{zy} & 0 \end{bmatrix} \tag{5}$$

The first four Fourier coefficients are calculated from these co- and quadrature spectra as follows:

$$\begin{aligned} a_1 &= \frac{Q_{xz}}{\sqrt{(C_{xx}+C_{yy})C_{zz}}} \\ b_1 &= \frac{Q_{yz}}{\sqrt{(C_{xx}+C_{yy})C_{zz}}} \\ a_2 &= \frac{C_{xx}-C_{yy}}{C_{xx}+C_{yy}} \\ b_2 &= \frac{-2C_{xy}}{C_{xx}+C_{yy}} \end{aligned} \tag{6}$$

These coefficients provide the approximation of the directional distribution of waves (Longuet-Higgins et al., 1965; Kuik et al., 1988):

$$D(\theta) = \frac{1}{\pi}\left(\frac{1}{2} + a_1\cos\theta + b_1\sin\theta + a_2\cos 2\theta + b_2\sin 2\theta\right) \tag{7}$$

From these coefficients, one can calculate parameters as spectral moments m_k, mean wave period T_{m0}, spectral width ν, mean direction θ, and directional spread σ (Krogstad et al., 1999):

$$\begin{aligned} m_k &= \int_f^\infty f^k S(f)df \\ T_{m0} &= \frac{m_0}{m_1} \\ \nu &= \sqrt{\frac{m_0 m_2}{m_1^2} - 1} \\ \theta(f) &= atan2\left(\frac{b_1(f)}{a_1(f)}\right) \\ \sigma_1(f) &= \sqrt{2\left(1 - \sqrt{a_1(f)^2 + b_1(f)^2}\right)} \end{aligned} \tag{8}$$

The wave spectra for the two measurement sets are structured in hourly time intervals and are automatically correlated and adjusted for time differences by the WavEval Tool. If spectra are given twice an hour as in the current study, the resulting hourly spectral values used in the comparison will be calculated from the combination of the values from the two spectra measured at most 30 min from the hour. For n number of spectra combined over an hour, the first five Fourier coefficients are calculated from each spectra's Fourier coefficients;

$$\begin{aligned} S(f)_{combined} &= \frac{\sum_{i=1}^n S_i(f)}{n} \\ a_1(f)_{combined} &= \frac{\sum_{i=1}^n S_i(f)a_{1,i}(f)}{\sum_{i=1}^n S_i(f)} \\ a_2(f)_{combined} &= \frac{\sum_{i=1}^n S_i(f)a_{2,i}(f)}{\sum_{i=1}^n S_i(f)} \\ b_1(f)_{combined} &= \frac{\sum_{i=1}^n S_i(f)b_{1,i}(f)}{\sum_{i=1}^n S_i(f)} \\ b_2(f)_{combined} &= \frac{\sum_{i=1}^n S_i(f)b_{2,i}(f)}{\sum_{i=1}^n S_i(f)} \end{aligned} \tag{9}$$

The spectra are organized in bins of frequency (here we use bandwidth 0.01 Hz) and wave energy (integrated over all directions). These bins are displayed as pixels in the energy versus frequency figures in this paper (see for example Fig. 11).

The zeroth moment for each of these bins is given as:

$$m_0(bin) = \int_f^{f+\Delta f} S(f)df \tag{10}$$

Here Δf is the frequency bandwidth of 0.01 Hz. The energy per bin (or pixel) is given on a logarithmic scale and is the energy density (unit m^2Hz^{-1}) multiplied with the frequency bin width (unit Hz). Hence the unit of the energy on the y-axis of the WavEval plots is m^2. The right y-axis, also logarithmic scale, displays the root mean square wave height, H_{RMS} per bin given as:

$$H_{RMS}(bin) = 2\sqrt{2}\sqrt{m_0(bin)} = 2\sqrt{2}\sqrt{\int_f^{f+\Delta f} S(f)df} \tag{11}$$

The significant wave height, H_{m0} per bin is given as:

$$H_{m0}(bin) = 4\sqrt{m_0(bin)} = 4\sqrt{\int_f^{f+\Delta f} S(f)df} \tag{12}$$

The different wave spectra will contribute to a sequence of values for comparison binned by both frequency and wave energy. The energy and H_{RMS} values on the y-axes correspond to an integration over a frequency bin and not over the full frequency range. Hence, these energies and height values will be lower than the equivalent values over the full spectrum. Over longer time periods (one month for example), one obtains observations from a wide range of sea states. Hence, many of the frequency and energy bins will have a statistically significant number of points for comparison. The plots generated show the statistical comparison between the measurements from two buoys; bias and root mean square error (RMSE). The comparisons are done based on the wave height and direction parameters using at least 10 hourly spectra per frequency/energy interval. Bias and RMSE values are given as numbers in each bin, either in percent difference or in degrees difference. To aid the reader, the bias and RMSE values are coloured according to the amount of difference, summarized in Table 1. RMSE values are calculated with bias removed.

Table 1
Colour description for the WavEval plots, bias and RMSE ranges.

	Colour	Percent height/Energy	Degrees
Bias	White	−5% to +5%	−5° to +5°
	Lightest red/blue	| 5% to 10% |	| 5°- 10° |
	Light red/blue	| 10% to 20% |	| 10°- 20° |
	Red/blue	> | 20% |	> | 20° |
RMSE	Green	< 15%	< 10°
	Yellow	15% to 25%	10°- 20°
	Orange	25% to 50%	20°- 30°
	Red	> 50%	> 30°

3. Results

The comparisons are done for time periods where the measurement setup for the buoys and sensors were constant (December 2017 to March 2018). Results are shown for the period December 6th 2017 to March 21st 2018 (both wave height and wave direction) and for March 5th to March 21st 2018 (evaluation of external compass correction for wave direction). For a small part of the measurement period, there were strong ocean currents for which the Waverider has limited data coverage as it is periodically submerged and stops transmitting data (above approximately 60–80 cm/s). Both the Tideland and EMM buoys transmit measurements also during periods of strong currents. The data used in the analysis are telemetered data. The validation of the MOTUS wave measurements relative to Waverider, is hence limited to periods with ocean currents below approximately 60–80 cm/s when the Waverider (telemetered) data are available.

3.1. Wave height

All comparisons presented for wave height are for the period December 2017 to March 2018, with a gap in second half of December because of irregular measurements and transmittance of data from Tideland and EMM. Fig. 8 compares time series of the significant wave height, H_{m0}, for MOTUS on Tideland and on EMM, and for Waverider.

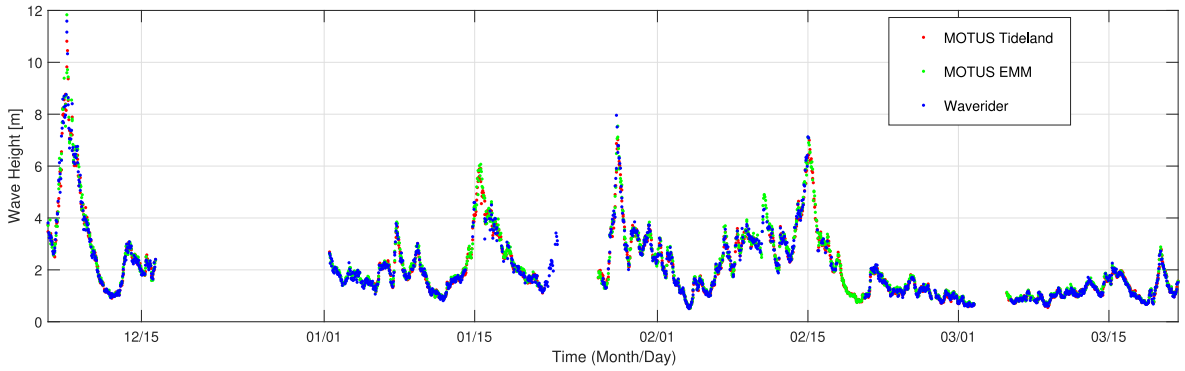

Fig. 8. Significant wave height, H_{m0}, integrated over frequencies 0.03–0.5 Hz. MOTUS on Tideland (red), on EMM (green), and Waverider (blue), December 6th 2017–March 21st 2018. (For interpretation of the references to colour in this figure legend, the reader is referred to the web version of this article.)

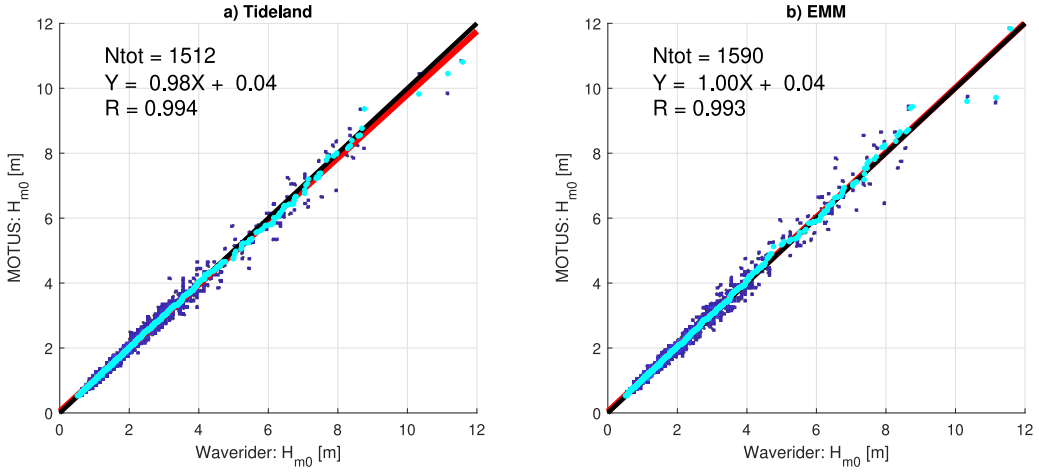

Fig. 9. Significant wave height, H_{m0}, integrated over frequencies 0.03–0.5 Hz (dark blue markers); 1:1 line (black), linear fit (red), Q–Q plot (light blue markers); (a) Tideland vs. Waverider, calculated mean bias −0.01 m. (b): EMM vs. Waverider, calculated mean bias 0.04 m. (For interpretation of the references to colour in this figure legend, the reader is referred to the web version of this article.)

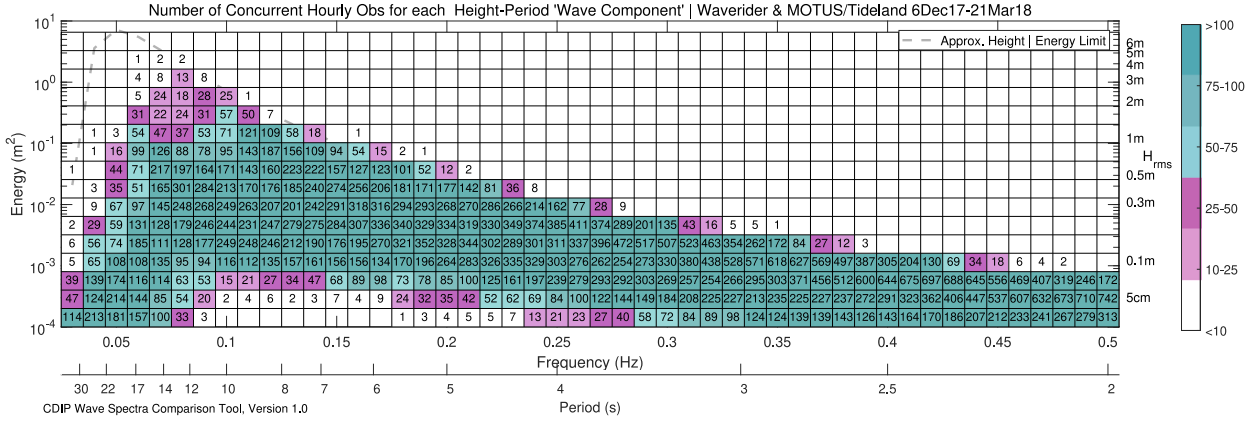

Fig. 10. Tideland vs. Waverider: Number of observations coloured and listed in each frequency/energy bin. Lower threshold for comparisons set to 10 number of concurrent observations. (For interpretation of the references to colour in this figure legend, the reader is referred to the web version of this article.)

H_{m0} is integrated over frequencies 0.03–0.5 Hz. One can observe that the period includes 4 storms with H_{m0} reaching 6 m or above. 46% of the Waverider data presented here have H_{m0} between 1 and 2 m; 32% of the data are between 2 and 4 m; and 7% are above 4 m.

Fig. 9 shows scatter plots (dark blue markers) of H_{m0} values of MOTUS on (a) Tideland and (b) EMM versus Waverider, with a total of 1512 and 1590 hourly data points, respectively. The black line shows the 1:1 ratio, and the red line shows the linear regression line between the measurements. For MOTUS on Tideland, the calculated mean bias is −0.01 m, and the correlation coefficient, R is found to be 0.994. The equivalent values for MOTUS on EMM are 0.04 m bias, and a R of 0.993. Also shown are Q–Q plots in light blue markers, i.e. the probability distributions of the test (MOTUS) and reference measurements (Waverider), since the measurements are not from exactly the same location.

The WaveEval Tool is used to compare the wave measurements of the MOTUS on Tideland and EMM to the Waverider in binned

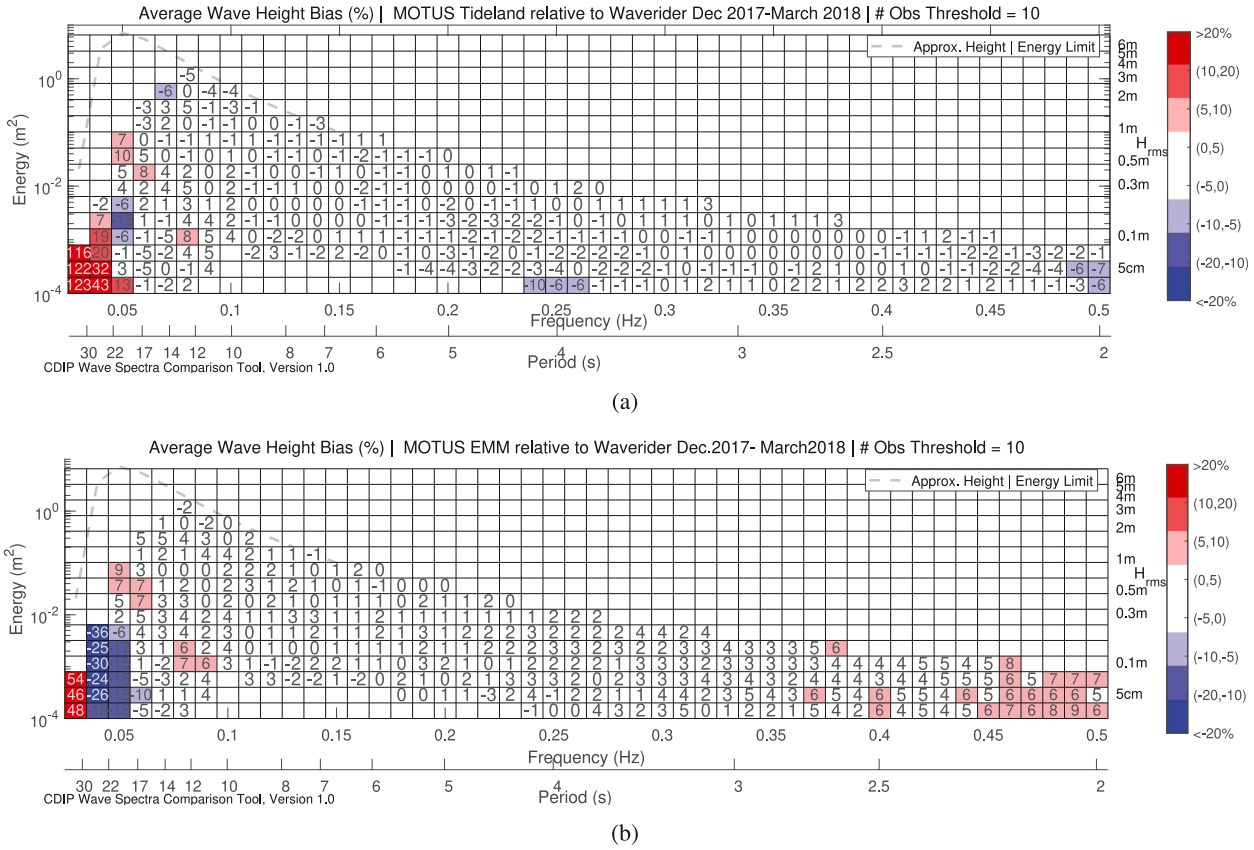

Fig. 11. Average Wave height bias (% of energy) listed in each frequency/energy bin and corresponding colour scale for (a) Tideland vs. Waverider, and (b) EMM vs Waverider. (For interpretation of the references to colour in this figure legend, the reader is referred to the web version of this article.)

frequency and energy intervals. Fig. 10 shows the number of concurrent hourly observations for Tideland and Waverider in the validation period, listed in each frequency/energy bin and colour coded to aid the reader. The lower threshold for comparisons is set to 10 hourly observations. EMM had equivalent numbers of concurrent hourly observations as Tideland for this period (not shown).

Bias and RMSE values are calculated for each frequency/energy bin, equivalent as was done for the scatter plot of the full frequency range (see Fig. 9). Fig. 11 shows the average wave height relative bias (unit percent of wave height) between Tideland (top) and EMM (bottom) relative to Waverider for each frequency/energy bin. For frequencies above 0.05 Hz, the bias is mainly below 5% (white boxes). Fig. 12 shows the equivalent RMSE values between Tideland/EMM and Waverider. If the RMSE was evaluated by using two identical and ideal wave sensors (no bias, no noise) and both sensors were situated at the same buoy at the same location and had exactly the same sampling scheme, you would have a RMSE that is 0. When moving the two sensors apart on separate identical buoys, they would no longer observe the same waves at the same time. The result would be an RMSE that is dependent on the distance between the two wave buoys. A similar effect would be observed if the sensor are localized on the same buoy, but with a sampling scheme that is not synchronized (e.g. if the measurement are interleaved in time). The wavefield has both spatial and temporal variability, so distance between sensors and sampling scheme are of interest when investigating the RMSE. In addition, the RMSE will be influenced by measurement variability (noise) of the two sensors in comparison. Numbers listed in each frequency/energy bin give the RMSE in percent of wave height. For frequencies above 0.05 Hz the RMSE values are below 25% (yellow) and below 15% (green) in some parts for frequencies above 0.1 Hz.

Table 2
Overview of H_{m0} comparisons between MOTUS sensors vs. Waverider for values integrated/evaluated over the full frequency range 0.03–0.5 Hz.

$\int df$: [0.03 – 0.5]Hz		N_{TOT}	Y = aX + b	Bias	R
H_{m0}	Tideland	1512	Y = 0.98 X + 0.04	−0.01 m	0.994
H_{m0}	EMM	1590	Y = 1.00 X + 0.04	0.04 m	0.993

Tables 2 and 3 show the overview of the wave height comparisons of MOTUS wave sensors onboard the navigational buoys Tideland and EMM versus Waverider. Table 2 summarizes the comparison of H_{m0} over the full frequency range. Table 3 provides an overview of the spectral comparisons of wave height measurements for different frequency intervals.

For the evaluation of the wave observations in periods of stronger ocean currents (above 60 cm/s), we have investigated variations in wave parameters as function of time. The comparisons have not been binned in frequency and energy due to limited data coverage of the Waverider buoy in periods of strong currents. Fig. 13 shows the wave height and current absolute speed for March 2018. Periods of missing data is easier to see from Fig. 14, which shows one of the periods of strong currents in early March 2018. The blue line is Waverider, and times with data are indicated by markers. MOTUS wave measurements are shown with orange (Tideland) and yellow (EMM) lines. Immediately before and after periods of data gaps of the Waverider buoy, the measured wave heights for the three different buoys agree well. There is no apparent difference compared to periods with weaker ocean currents. In periods of strong currents, there is no noticeable disagreement between the wave height observations from EMM and Tideland.

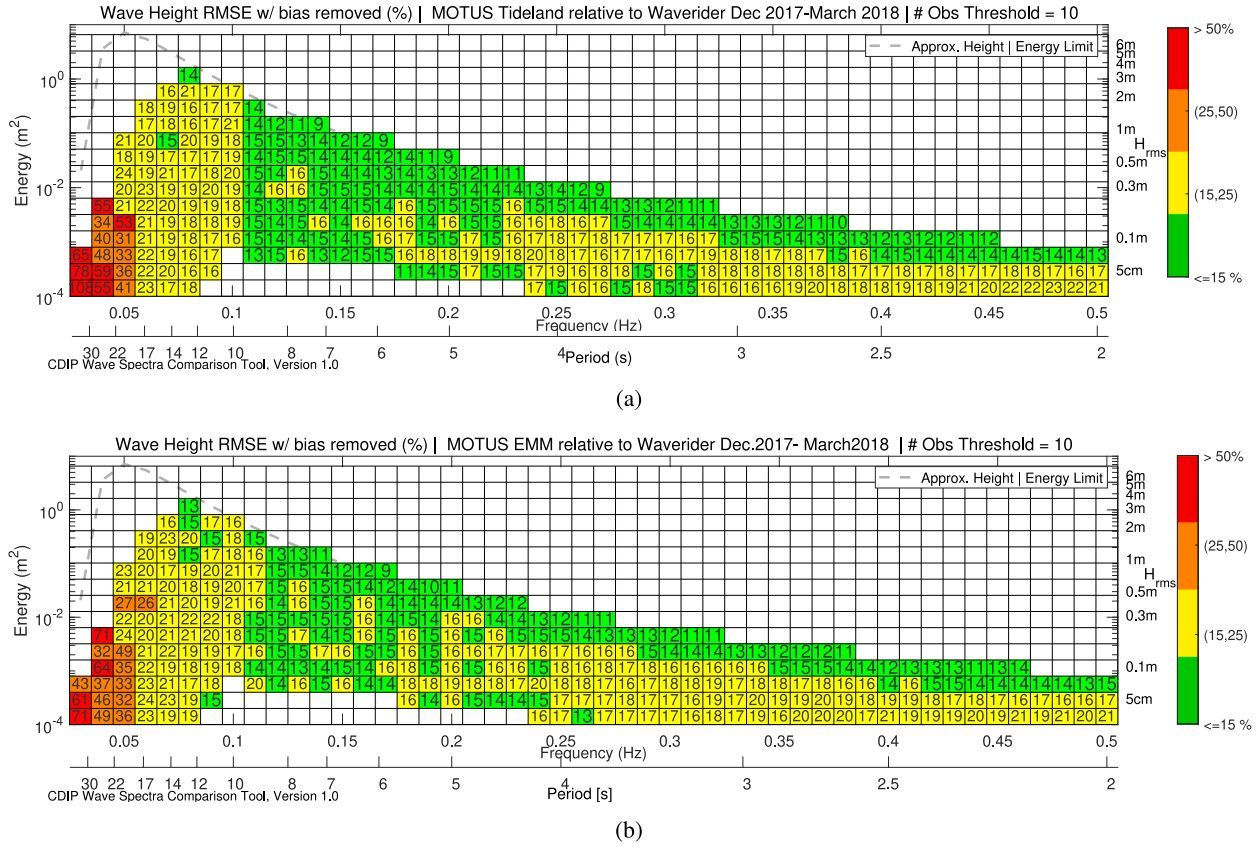

Fig. 12. Average Wave height RMSE (% of energy) listed in each frequency/energy bin and corresponding colour scale for the period December 6th 2017–21st March 2018, for MOTUS on (a) Tideland, and (b) EMM vs Waverider. (For interpretation of the references to colour in this figure legend, the reader is referred to the web version of this article.)

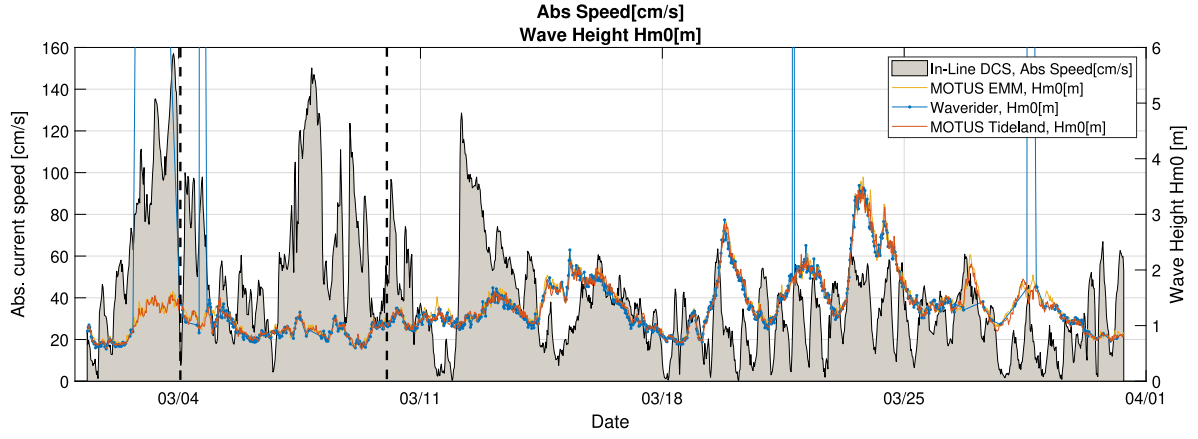

Fig. 13. Wave height H_{m0} [m] (right y-axis) from Waverider (blue), MOTUS sensor on EMM (yellow), MOTUS sensor on Tideland (orange), and absolute current speed [cm/s] from in-line DCS sensor (black/grey, left y-axis). Time period: March 5th–21st, 2018. Vertical dashed lines delimit the period shown in Fig. 14. (For interpretation of the references to colour in this figure legend, the reader is referred to the web version of this article.)

3.2. Wave direction

Comparison of MOTUS wave sensors onboard Tideland and EMM for December 2017 to March 2018 are presented in the following section. Also shown are comparisons in March 2018 for the second MOTUS wave sensor onboard EMM when external compass was enabled for this sensor.

Fig. 15 shows the time series of the mean wave direction, (D_{mean}, unit degrees) for Tideland, EMM with and without external compass correction, and Waverider. Here the mean direction is evaluated over frequencies 0.03–0.5 Hz from the first order Fourier components (a_1 and b_1). Fig. 16(a) shows the mean wave direction for the same period with Tideland versus Waverider, a total of 1512 data points. The calculated mean bias is 1.4 degrees, and the correlation coefficient, R, between the mean wave direction first order wave components is found to be 0.967. Fig. 16(b) shows the same comparison only with data points where wave height H_{m0} was greater than or equal to 2 m (MOTUS, Tideland H_{m0} values), giving a total of 591 data points. Calculated mean bias is 1.2 degrees, and correlation coefficient R is equal to 0.989. Equivalent comparisons for EMM versus Waverider for the same period are shown in Fig. 16(c). For this period, the second MOTUS sensor on EMM had disabled the external compass corrections. The

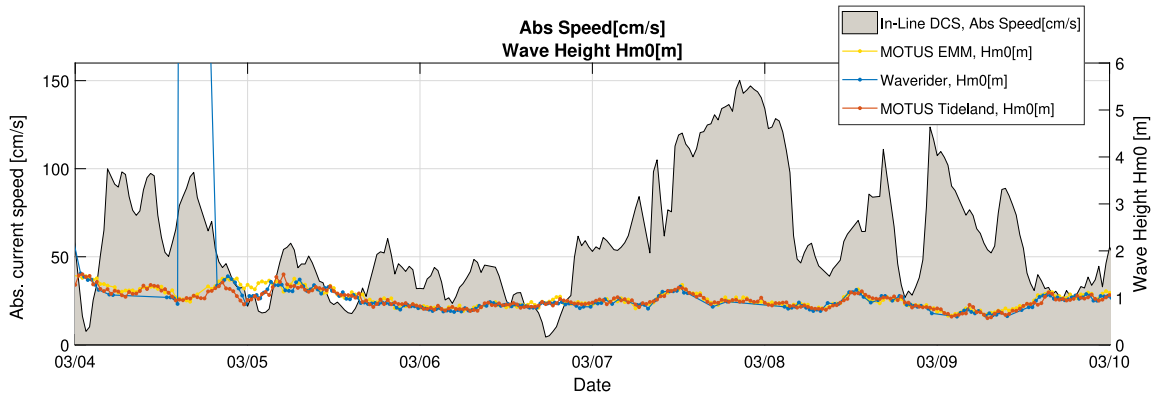

Fig. 14. Same as Fig. 13 for the period 4th to 9th March.

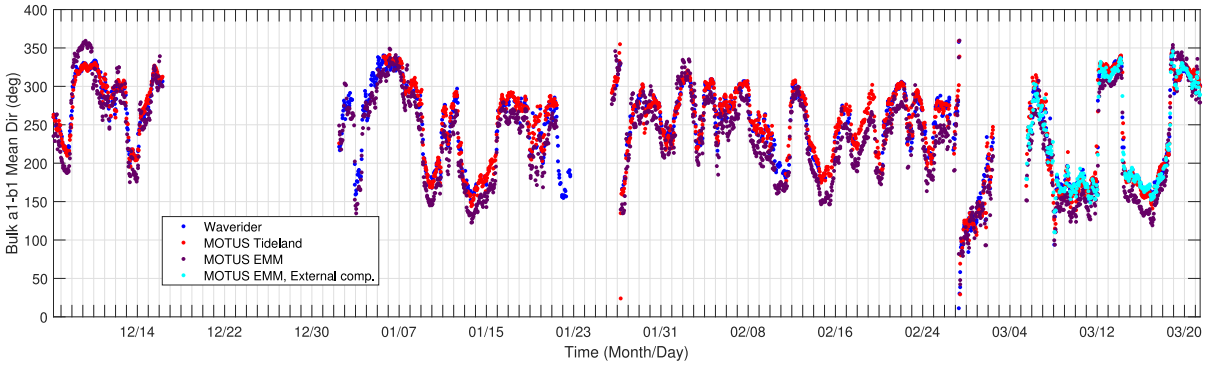

Fig. 15. Tideland vs. Waverider, December 2017–March 2018: mean wave direction (calculated from a1 and b1 first order wave parameters). (For interpretation of the references to colour in this figure legend, the reader is referred to the web version of this article.)

Table 3
Overview of the general trend for bias and RMSE for spectral validation of wave height from the MOTUS sensors vs. Waverider. E_{HIGH} and E_{LOW} means the higher and lower energy bins for the relevant frequency intervals.

		Bias			RMSE		
	Frequency [Hz]	< 0.05	0.05-0.45	0.45-0.5	< 0.05	0.05-0.1	> 0.1
Height	Tideland	> 20%	< |5%|	< |7%|	25% - >50% ($E<10^{-2}m^2$)	15%–25%	< 15% E_{HIGH} 15%–25% E_{LOW}
Height	EMM	<-20%	< |5%|	5%–10%	25% - >50% ($E<10^{-2}m^2$)	15%–25%	< 15% E_{HIGH} 15%–25% E_{LOW}

Table 4
Overview of bulk wave direction (a1, b1 first order wave components) comparisons between MOTUS sensors vs. Waverider for values integrated/evaluated over the full frequency range 0.03–0.5 Hz.

$\int df$: [0.03 – 0.5] Hz		N_{TOT}	Y = aX + b	Bias	R
D_{mean}	Tideland	1512	Y = 0.99 X + 3.54	1.4 deg	0.967
D_{mean}	Tideland (Hs >= 2 m)	591	Y = 1.01 X – 0.90	1.2 deg	0.989
D_{mean}	EMM	1590	Y = 1.06 X – 30.5	–15 deg	0.951
D_{mean}	EMM external compass	342	Y = 0.98 X + 1.95	–2.8 deg	0.991

calculated mean bias is –15 degrees, and the correlation coefficient, R is found to be 0.951. Fig. 16(d) shows the comparisons of mean wave direction for MOTUS sensor on EMM for 5th–21st March 2018 (number of coincident hourly spectra $N = 342$). For this period, the MOTUS on EMM had enabled external compass corrections. The calculated mean bias is –2.8 degrees, and the correlation coefficient R is improved to 0.991.

As for wave height, comparison of wave direction is also performed in smaller frequency and energy intervals where bias and RMSE values are calculated for each bin. Fig. 17 shows the numbers of concurrent hourly observations per bin for EMM and Waverider for the shorter period March 2018 with external compass enabled (see equivalent Fig. 10 for Tideland, December 2017–March 2018). Total number of comparisons, N_{tot} are listed in Fig. 16 for the different sets of comparison. Fig. 18 shows the average wave direction bias (unit degrees) between (a) MOTUS on Tideland and Waverider in the period December 2017 to March 2018; (b) MOTUS on EMM with external compass correction versus Waverider for March 2018, and (c) MOTUS on EMM with external compass correction versus MOTUS on Tideland, March 2018. For frequencies between 0.05 Hz and 0.45 Hz, the MOTUS on Tideland shows bias compared to Waverider mainly below 5 degrees (white) and below 10 degrees for lower energies (lightest red or lightest

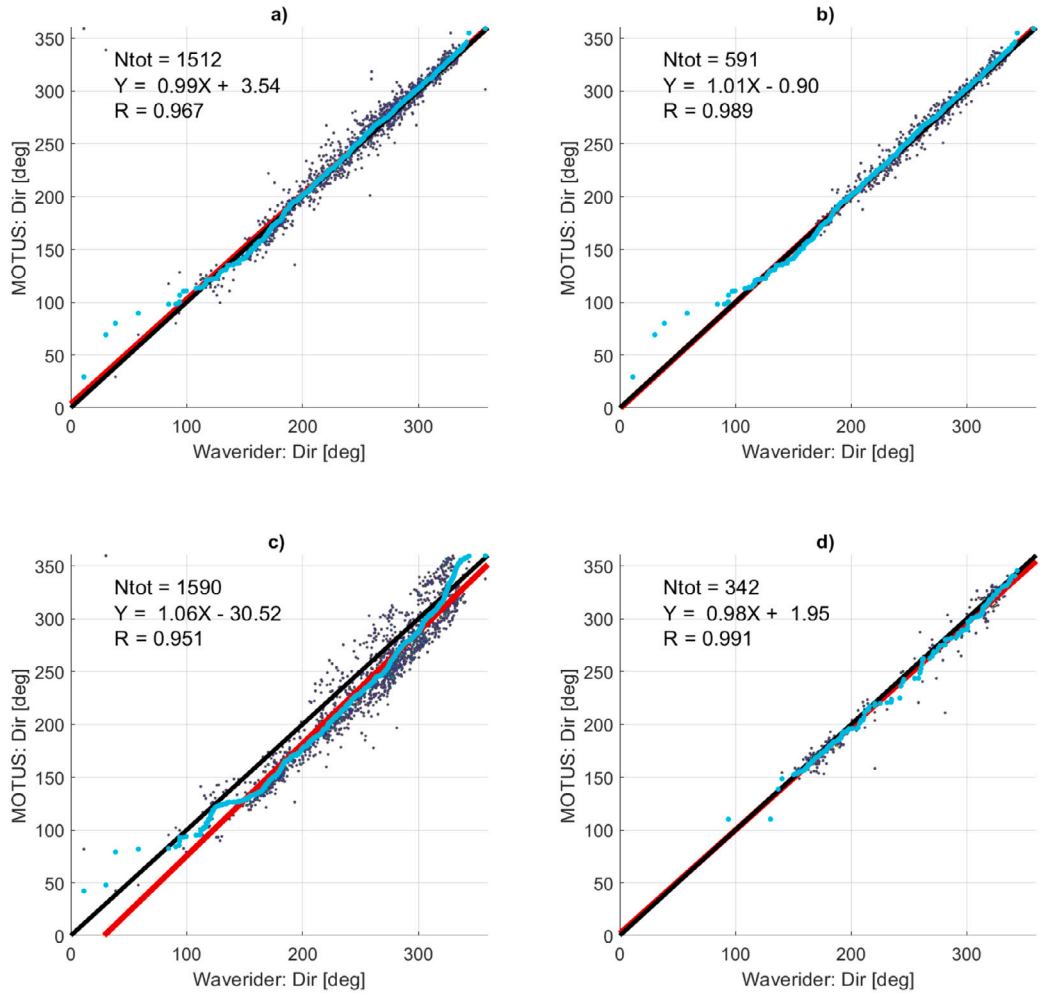

Fig. 16. Mean wave direction first order wave components (dark blue markers); 1:1 line (black), linear fit (red), Q–Q plot (light blue markers), December 2017–March 2018; (a) Tideland vs. Waverider (all data points), Calculated mean bias 1.4 degrees.; (b) Tideland vs. Waverider (H_{m0} >= 2 m), Calculated mean bias 1.2 degrees; (c) EMM vs. Waverider (External compass disabled), Calculated mean bias −15 degrees.; (d) EMM vs. Waverider (External compass enabled), March 5th–21st, 2018; Calculated mean bias −2.8 degrees. (For interpretation of the references to colour in this figure legend, the reader is referred to the web version of this article.)

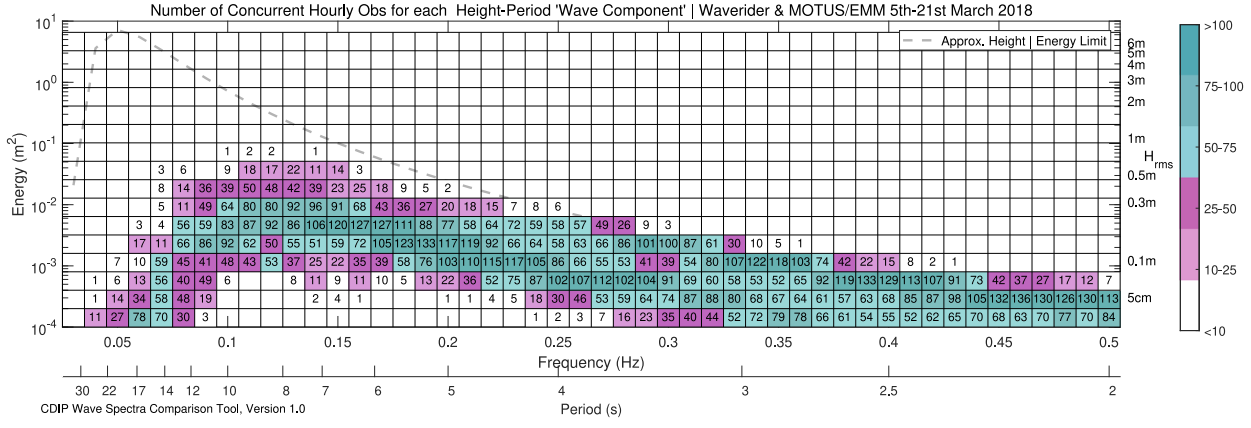

Fig. 17. EMM vs. Waverider, March 2018: Number of observations coloured and listed in each frequency/energy bin. Lower threshold for comparisons set to 10 number of coincidental observations. (For interpretation of the references to colour in this figure legend, the reader is referred to the web version of this article.)

blue). Fig. 19 shows the equivalent RMSE values between MOTUS on Tideland, MOTUS on EMM and Waverider. For frequencies above 0.05 Hz and energy bins above 10^{-3} m^2, the RMSE values for Tideland vs. Waverider are mainly below 20 degrees (yellow) and for the higher energies (above 10^{-2} m^2) also below 10 degrees (green). For EMM the MOTUS sensor with external compass correction show similar pattern in frequency/energy bins as for the Tideland MOTUS results when comparing to Waverider (bias Fig. 18b and RMSE Fig. 19b). However, with

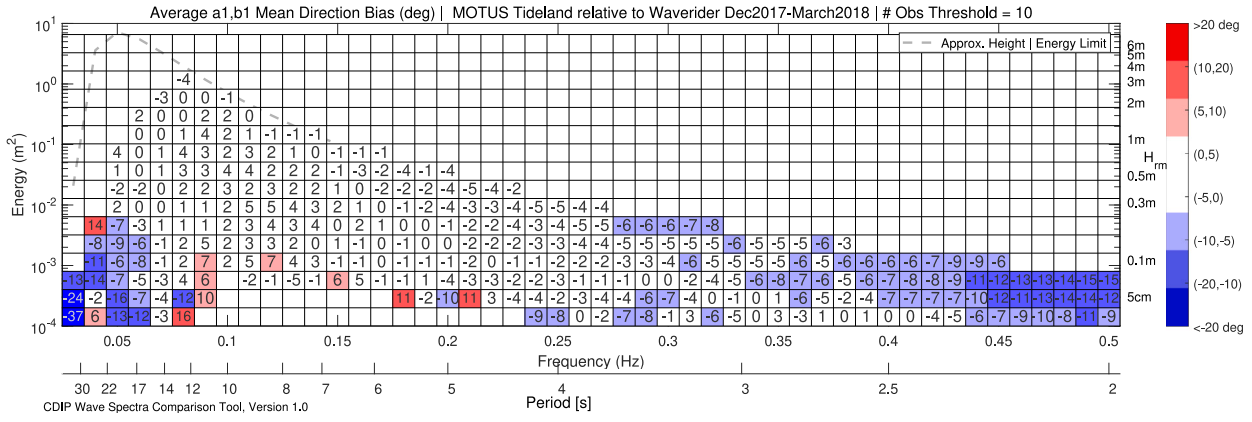

(a)

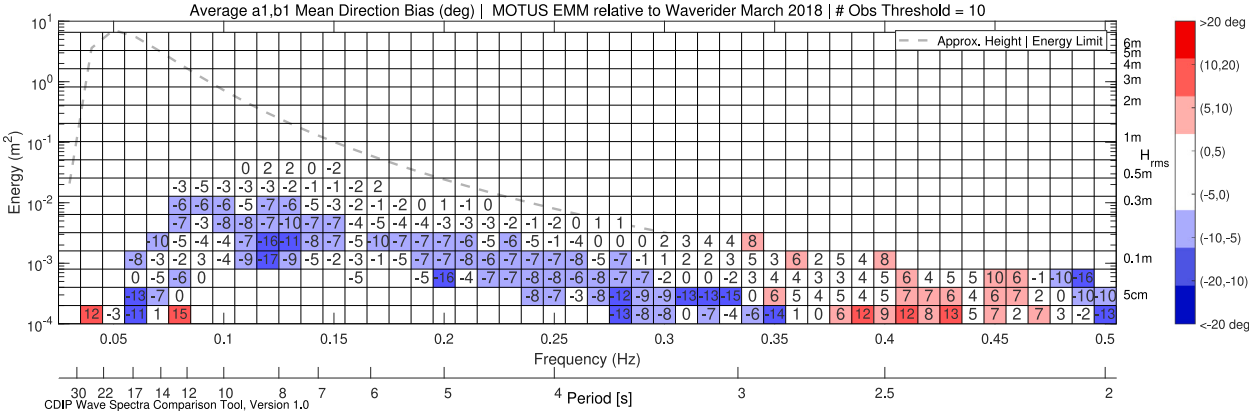

(b)

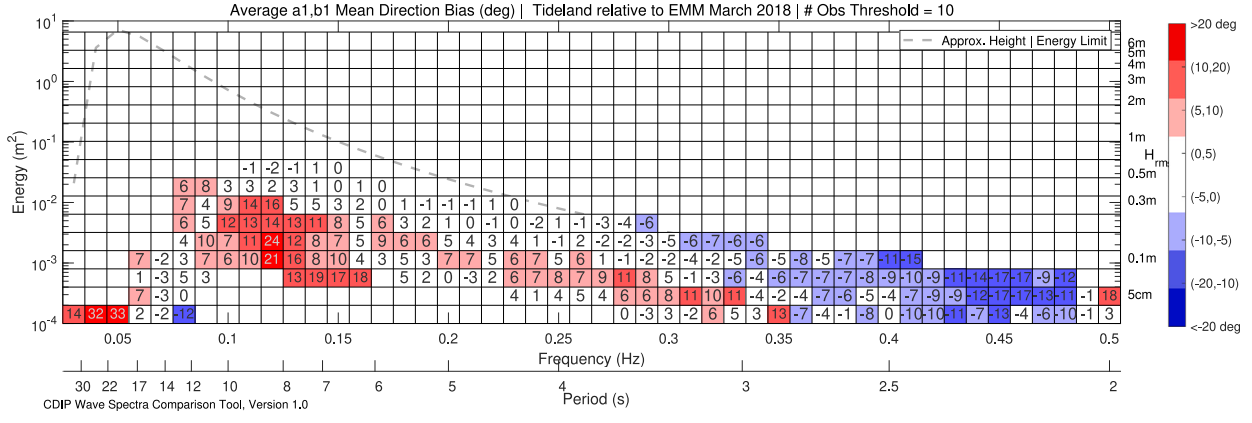

(c)

Fig. 18. Mean direction bias (degrees) listed in each frequency/energy bin and corresponding colour scale. (a) MOTUS on Tideland vs. Waverider, December 6th 2017–March 21st 2018; (b) MOTUS on EMM (external compass enabled) vs. Waverider, March 2018; (c) MOTUS on EMM (external compass enabled) vs. MOTUS on Tideland, March 2018. (For interpretation of the references to colour in this figure legend, the reader is referred to the web version of this article.)

a slightly enhanced bias for some parts of the spectra. We have also compared MOTUS on EMM vs. Tideland for March 2018 (bias Fig. 18c and RMSE Fig. 19c) as for EMM compared to Waverider. Here there are regions of elevated bias and RMSE values for frequencies between 0.1 and 0.2 Hz (energy per bin below 10^{-2} m^2). These comparisons also include periods of stronger currents, when both EMM and Tideland transmitted data (Figs. 20 and 21). Some of the deviation is also evident when comparing MOTUS to Waverider for both buoys. However, for the 0.1–0.2 Hz frequency range, the elevated bias and RMSE values could be due to comparisons of periods with strong currents, where the wave direction measurements show larger variations.

Tables 4 and 5 show an overview of the directional comparison of MOTUS wave sensors onboard the navigational buoys Tideland and EMM versus Waverider. Table 4 summarizes the comparison of mean wave direction over the full frequency range. Table 5 provides an overview of the spectral comparisons of mean direction wave measurements (first order) for different frequency intervals.

As for wave height, the wave directional measurements are evaluated in periods of stronger ocean currents (above 60 cm/s) without

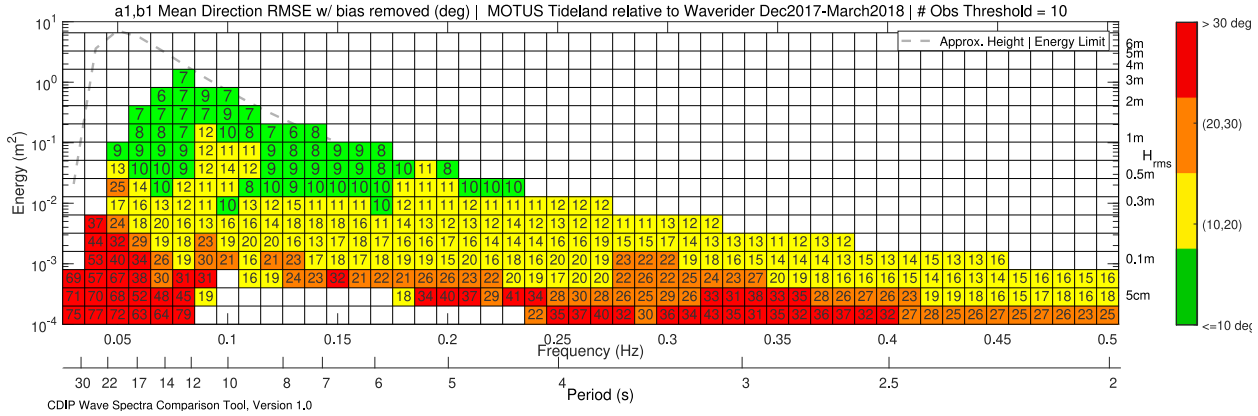

(a)

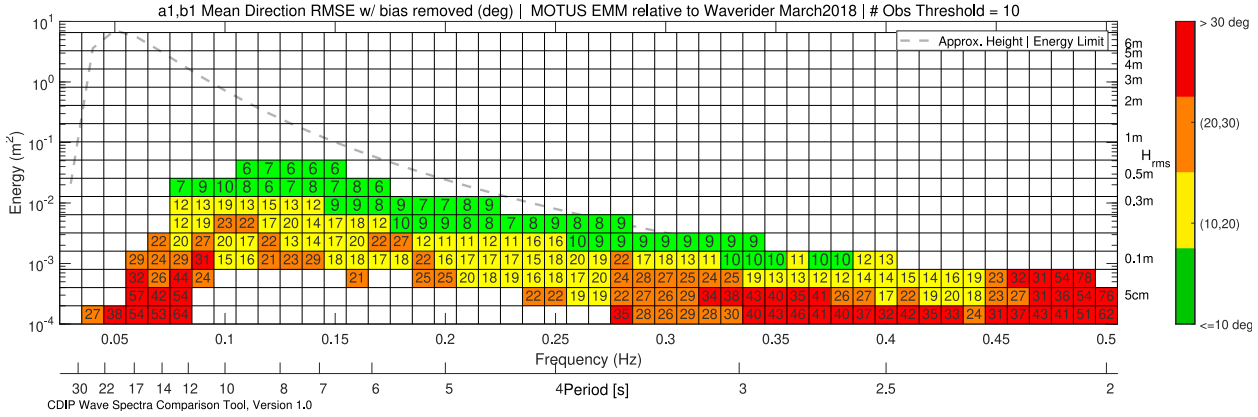

(b)

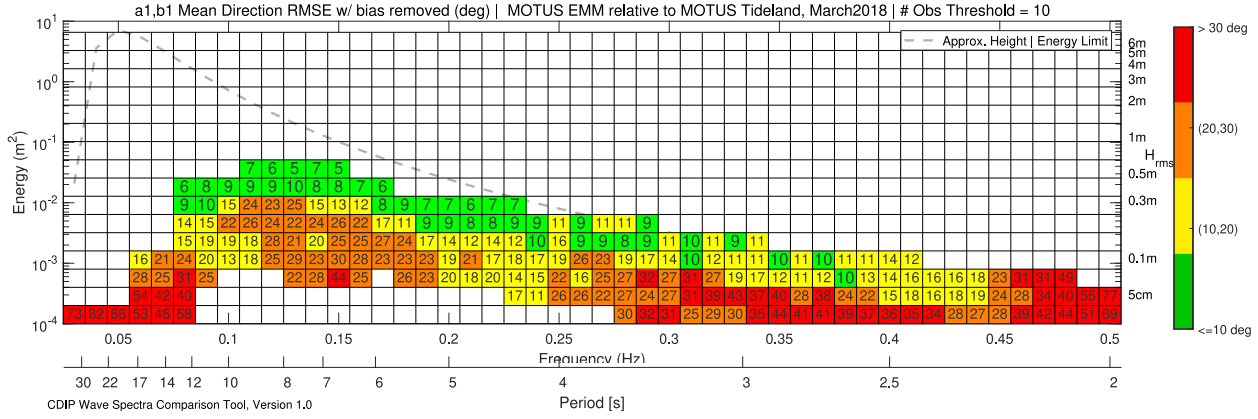

(c)

Fig. 19. Mean direction RMSE (degrees) listed in each frequency/energy bin and corresponding colour scale. (a) MOTUS on Tideland vs. Waverider, December 6th 2017–March 21st 2018; (b) MOTUS on EMM (external compass enabled) vs. Waverider, March 2018; (c) MOTUS on EMM (external compass enabled) vs. MOTUS on Tideland, March 2018. (For interpretation of the references to colour in this figure legend, the reader is referred to the web version of this article.)

binning in frequency and energy. Again, the measured wave directions agree well immediately before and after periods of data gaps of the Waverider buoy, with no apparent difference compared to periods with lower ocean currents. Fig. 20 shows the wave mean direction and current absolute speed for March 2018. For strong currents (> 80 cm/s) the wave direction measurements also for the Tideland and EMM buoy show strong variations (see especially the start of the period in Fig. 20). Periods of missing data is easier to see from Fig. 21, which shows one of the periods of strong currents, from 7th to 10th March 2018. The blue line is Waverider, and times with data are indicated by markers. MOTUS wave measurements are shown as orange lines (Tideland),

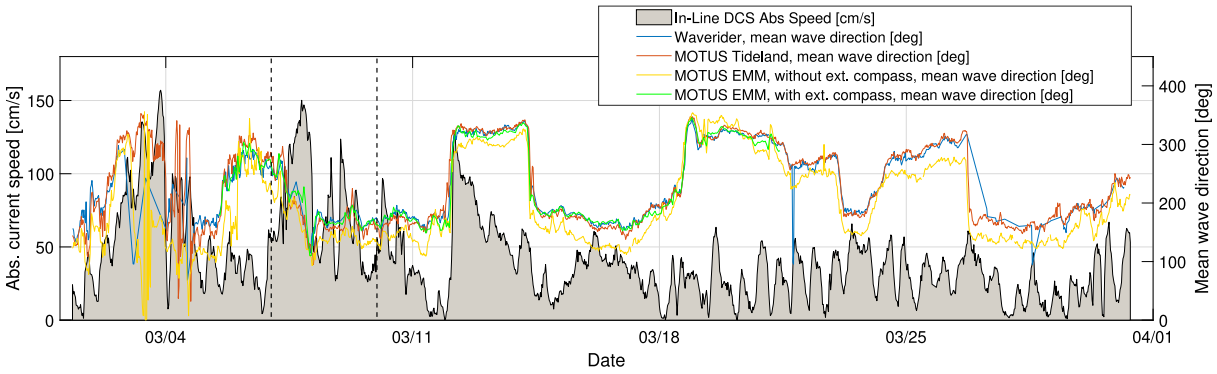

Fig. 20. Wave mean direction [deg] (right y-axis) from Waverider (blue), MOTUS sensor on Tideland (orange) and EMM (yellow without and green with external compass correction), and absolute current speed [cm/s] from in-line DCS sensor (black/grey, left y-axis). March 2018. (For interpretation of the references to colour in this figure legend, the reader is referred to the web version of this article.)

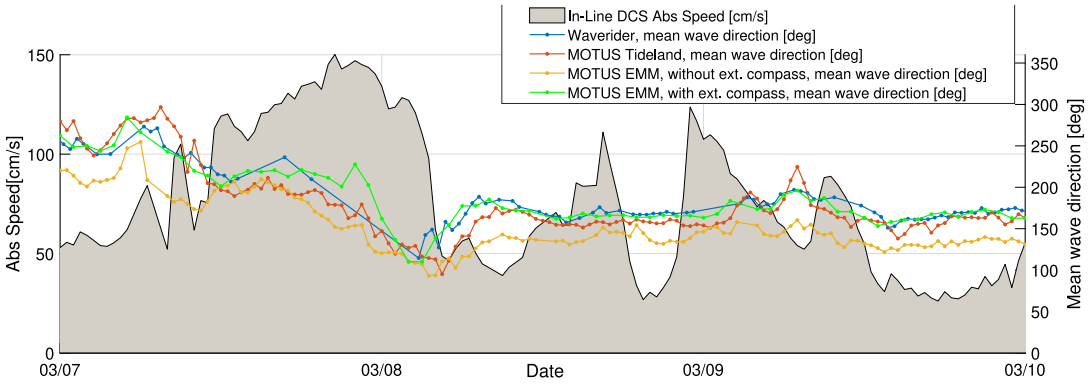

Fig. 21. Same as Fig. 20 (vertical dashed lines) for the period 7th to 10th March.

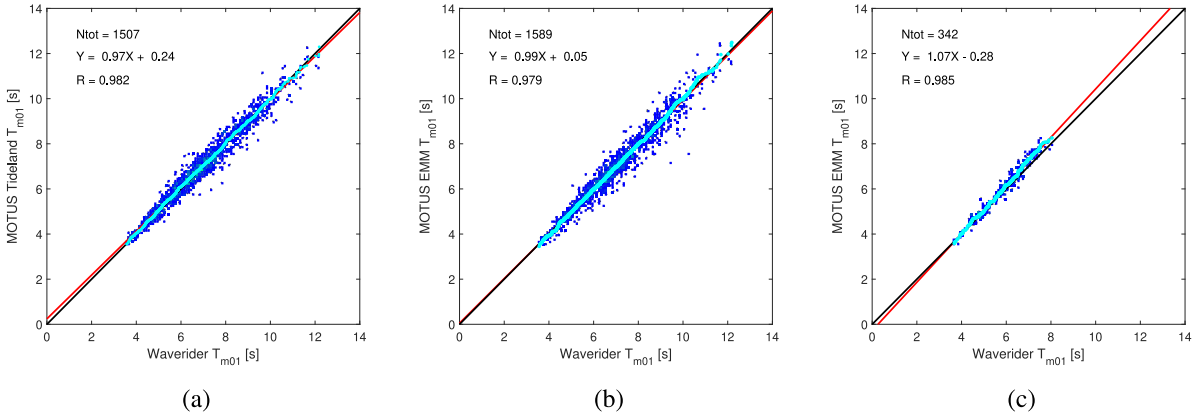

Fig. 22. Mean period (blue squares), 1:1 line (black), linear fit (red), and Q–Q plot (light blue) (a) Tideland vs. Waverider Dec.2017–March 2018, bias 0.03 s, (b) EMM vs Waverider Dec.2017–March 2018, bias −0.03 s, and (c) EMM w/external compass vs Waverider March 2018, bias 0.13 s. (For interpretation of the references to colour in this figure legend, the reader is referred to the web version of this article.)

yellow lines (EMM without external compass correction), and green lines (EMM with external compass correction).

3.3. Mean period, spectral width, and directional spreading

In this section additional statistical metrics for the wave buoy comparisons are presented. Fig. 22 shows the mean period of MOTUS on Tideland and EMM relative to Waverider in the period December 2017 to March 2018, and for MOTUS on EMM with external compass enabled relative to Waverider in March 2018. Linear approximation and correlation coefficients R of the data are shown in each plot. Also shown in the plots are the Q–Q distributions (light blue). Fig. 23 shows equivalent comparisons of the spectral width, and Fig. 24 shows the comparison of directional spread (first order). All parameters are evaluated over frequencies between 0.03–0.5 Hz.

3.4. Frequency spectral results

The mean energy, direction, and directional spread are presented here as functions of frequency. Fig. 25 shows the mean of the energy spectra of Waverider and MOTUS on Tideland and EMM in the period December 2017 to March 2018 (solid lines), and the mean energy spectra only evaluated for the wave energies above the 90th percentile (dashed lines). Fig. 26 shows the equivalent plot for MOTUS on EMM

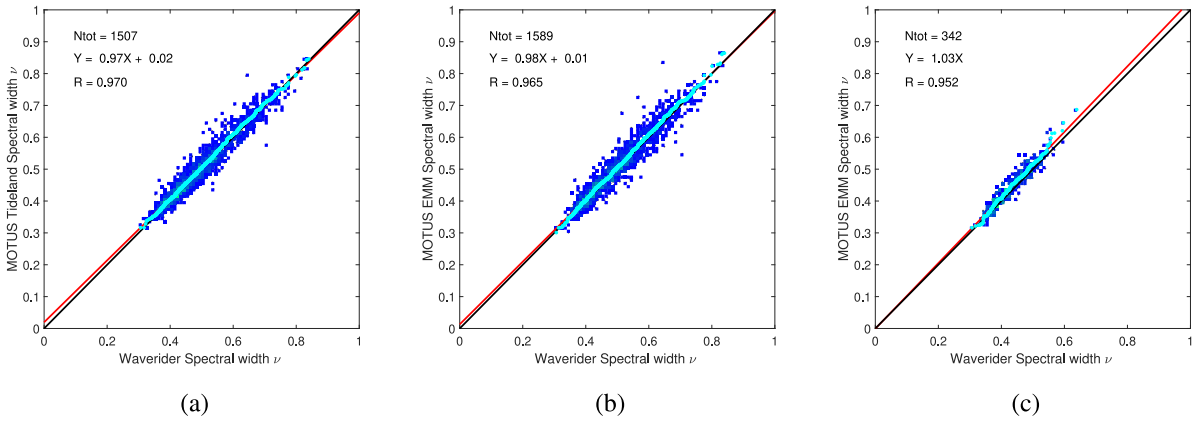

Fig. 23. Spectral width (blue squares), 1:1 line (black), linear fit (red), and Q–Q plot (light blue) (a) Tideland vs. Waverider Dec.2017–March 2018, bias 0.0, (b) EMM vs Waverider Dec. 2017–March 2018, bias 0.5, and (c) EMM w/external compass vs Waverider March 2018, bias 0.01. (For interpretation of the references to colour in this figure legend, the reader is referred to the web version of this article.)

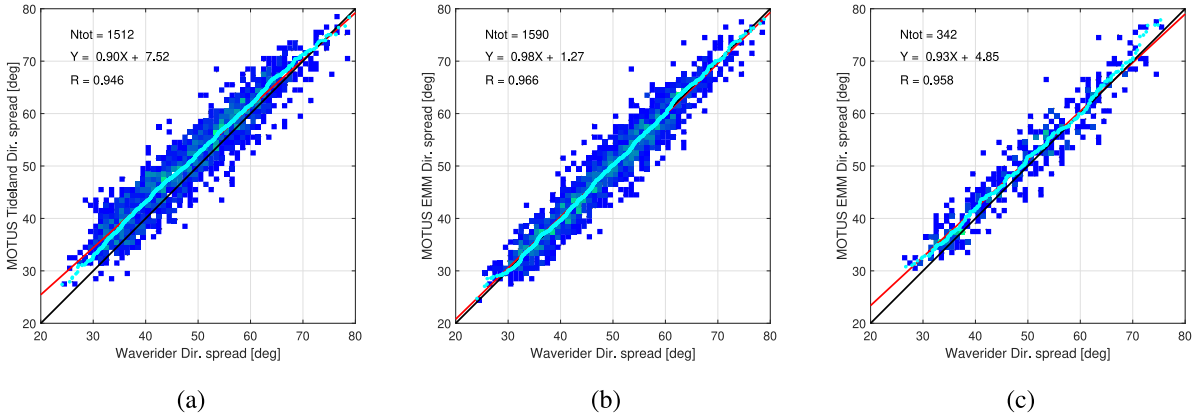

Fig. 24. Directional spread, first order (blue squares), 1:1 line (black), linear fit (red), and Q–Q plot (light blue) (a) Tideland vs. Waverider Dec.2017–March 2018, bias 2.51 deg, (b) EMM vs Waverider Dec. 2017–March 2018, bias 0.08 deg, and (c) EMM w/external compass vs Waverider March 2018, bias 1.3 deg. (For interpretation of the references to colour in this figure legend, the reader is referred to the web version of this article.)

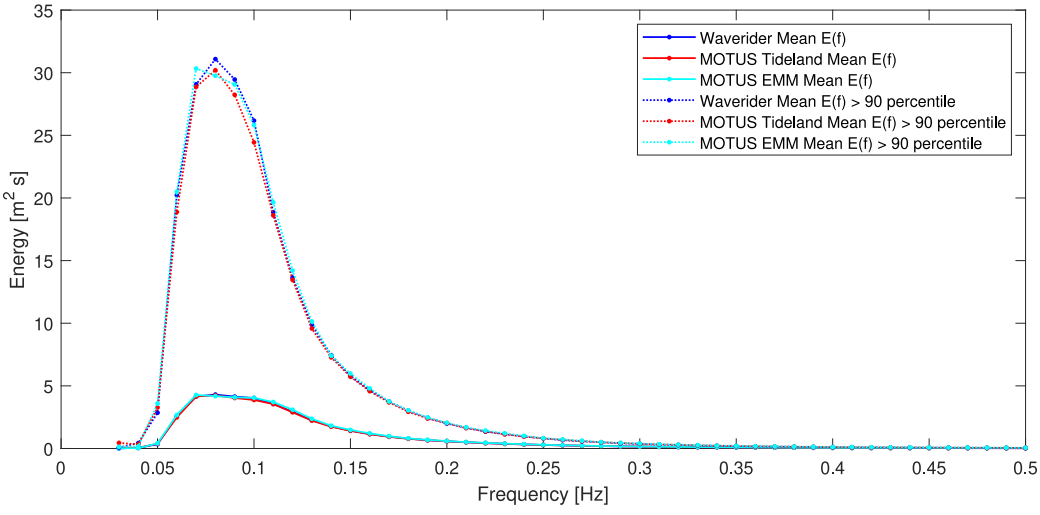

Fig. 25. Mean energy spectra for Waverider (blue), MOTUS on Tideland (red) and on EMM (cyan) Dec. 2017–March 2018. Also shown are the mean energy spectra for wave energies above the 90th percentile (dotted lines). (For interpretation of the references to colour in this figure legend, the reader is referred to the web version of this article.)

with external compass enabled for March 2018. The wave energies are significantly larger for the December to March period. The comparisons for March 2018 were included for the evaluation of external compass correction for the MOTUS sensor on EMM. Fig. 27 shows the mean difference in the bulk directions for MOTUS on Tideland and on EMM (with and without external compass) compared to Waverider, and

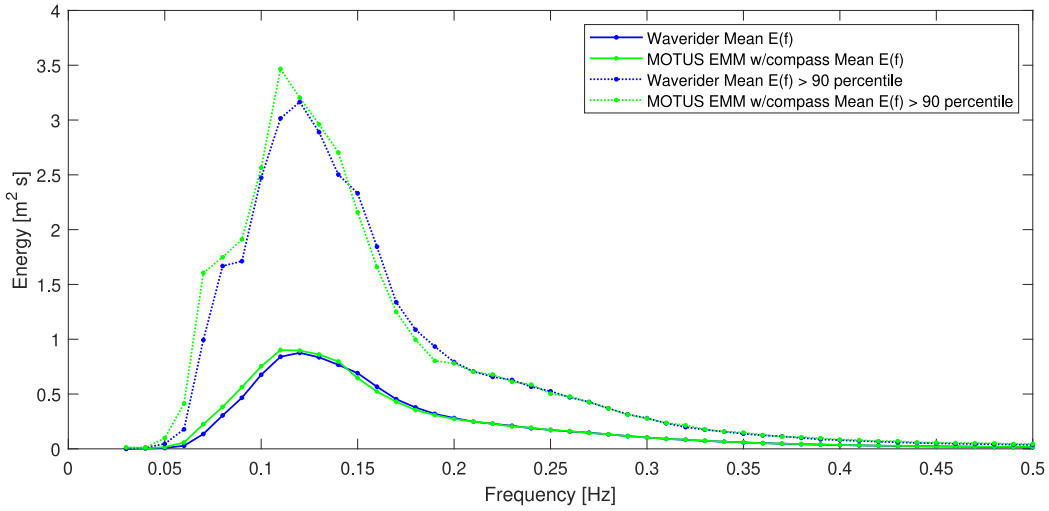

Fig. 26. Mean energy spectra for Waverider (blue) MOTUS on EMM with external compass (green) March 2018. Also shown are the mean energy spectra for wave energies above the 90th percentile (dotted lines). (For interpretation of the references to colour in this figure legend, the reader is referred to the web version of this article.)

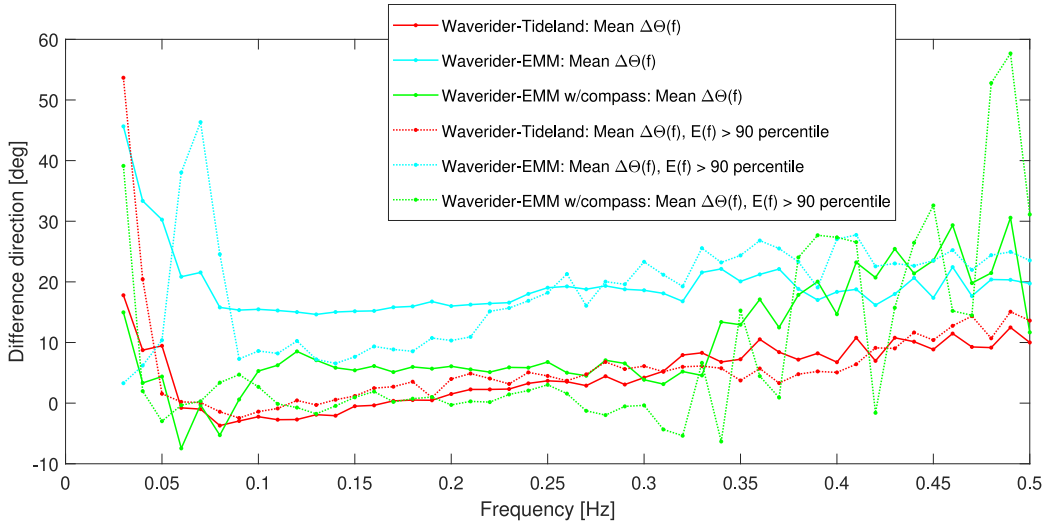

Fig. 27. Difference in mean direction MOTUS on Tideland (red) and on EMM (cyan) compared to Waverider Dec. 2017–March 2018, and MOTUS w/external compass on EMM (green) compared to Waverider March 2018. Also shown are the difference direction spectra for wave energies above the 90th percentile (dotted lines). (For interpretation of the references to colour in this figure legend, the reader is referred to the web version of this article.)

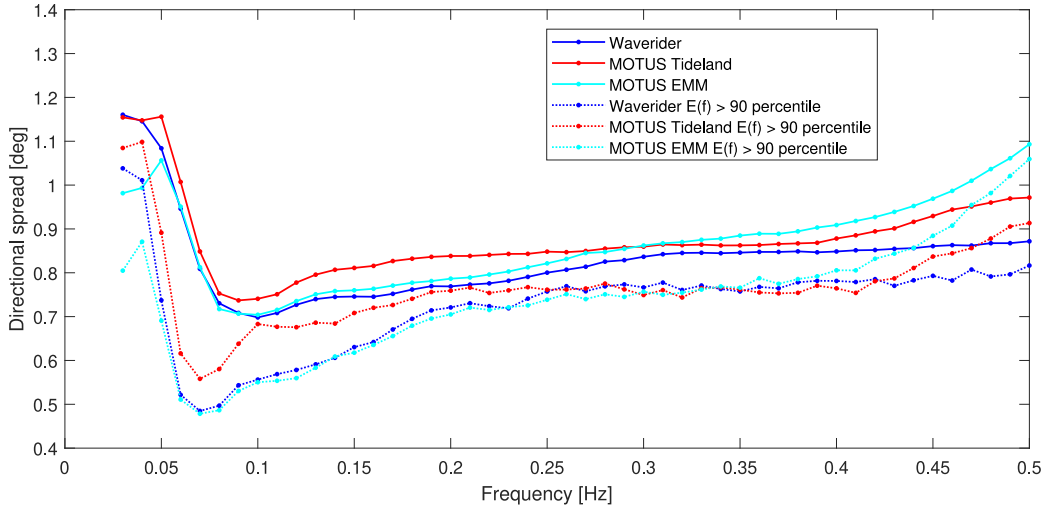

Fig. 28. Directional spread for Waverider (blue), MOTUS on Tideland (red) and on EMM (cyan) Dec. 2017–March 2018. Also shown are the directional spread spectra for wave energies above the 90th percentile (dotted lines). (For interpretation of the references to colour in this figure legend, the reader is referred to the web version of this article.)

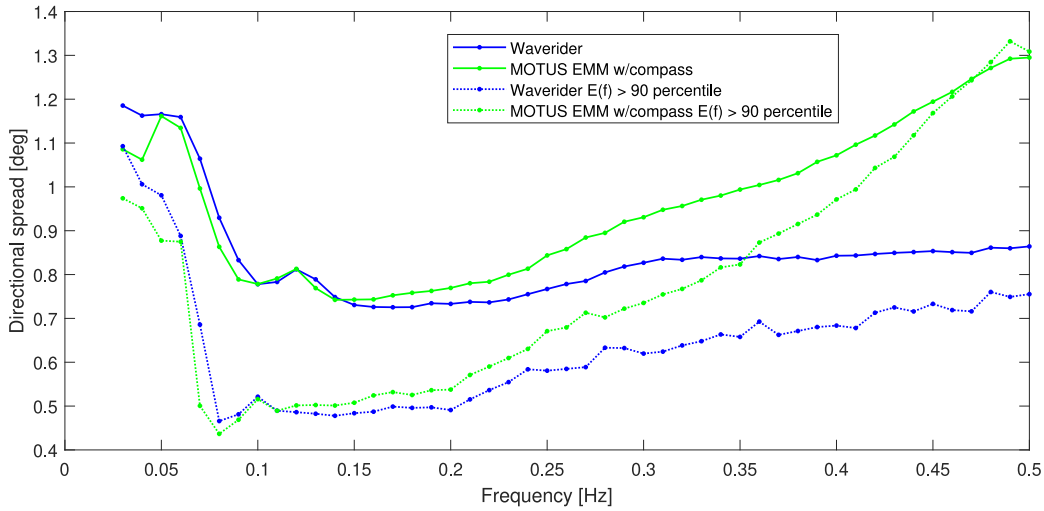

Fig. 29. Directional spread for Waverider (blue), MOTUS on EMM with external compass (green) March 2018. Also shown are the directional spread spectra for wave energies above the 90th percentile (dotted lines). (For interpretation of the references to colour in this figure legend, the reader is referred to the web version of this article.)

Table 5
Overview of the general trend for bias and RMSE for spectral validation of the mean direction wave measurements (first order) from MOTUS sensors vs. Waverider. E_{HIGH} and E_{LOW} means the higher and lower energy bins for the relevant frequency intervals.

		Bias			RMSE		
	Frequency [Hz]	< 0.05	0.05-0.45	0.45-0.5	< 0.05	0.05-0.1	> 0.1
D_{mean}	Tideland	< −10 deg	< |5 deg|	−6 to -20deg (f>0.4 Hz)	> 30 deg	6–20 deg (E>$10^{-3}m^2$)	10–20 deg E_{HIGH} 20–30 deg E_{LOW}
D_{mean}	EMM external compass	No data	−10 to 0deg	< |10%|	> 30 deg	6–20 deg (E>$10^{-3}m^2$)	10–20 deg E_{HIGH} > 30 deg E_{LOW}

for the mean difference evaluated for wave energies above the 90th percentile (dashed lines). For the frequencies where the wave energies are higher (see Figs. 26 and 27), the mean differences in direction are less than 5 degrees for MOTUS on Tideland, and less than 10 degrees for MOTUS on EMM with external compass enabled, and lower than 5 degrees for the mean difference also of EMM (with compass) for the 90% highest energies (dashed green line). Fig. 28 shows the directional spread as function of frequency for Waverider and MOTUS on Tideland and EMM, December 2017 to March 2018 (mean of all comparisons, and mean for wave energies above the 90th percentile). Fig. 29 shows the equivalent plot for Waverider and MOTUS on EMM with external compass enabled for March 2018.

3.5. Comparisons made in the development period

Comparisons have also been made in the development period (February 2017 to December 2017) with a pre-release firmware version. These results are included in the supplementary material. In this period different mooring solutions for the Tideland buoy were compared, and it was found that both wave height and wave direction bias and RMSE were not significantly different for the cases of elastic and rope mooring. For high energy waves, as seen in December 2017, the comparisons to Waverider show low bias values for wave height. Thus, there is no sign of rope mooring being insufficient for high waves. Comparisons were also done for Tideland with and without added weight of approximately 30 kg. There were no indications that the extra weight affected the wave measurements significantly.

4. Discussion

In this validation study, comparisons have been done between MOTUS sensors mounted on either a Tideland navigational buoy or an EMM coastal buoy and the reference represented by a Waverider buoy. The MOTUS sensors have been validated both for specific wave height and mean direction for the frequency range 0.03–0.5 Hz, and for spectral frequency and energy bins using the WavEval tool (Jensen et al., 2011; Alliance for Coastal Technologies, 2007; Luther et al., 2013; Cavaleri et al., 2018). Note that both Waverider and MOTUS sensors provide measurements higher than 0.5 Hz. The comparisons show that both the Tideland navigational buoy and the EMM coastal buoy with MOTUS wave sensors provide good measurements of wave heights based on wave energy at frequencies above 0.05 Hz. For the most of the frequency/energy bins, the bias for wave height is below 5%. The RMSE values for wave height for frequency bins above 0.05 Hz are below 25%. This variability could be partially due to wave variability at the different locations of the buoys. The correlation coefficient for the total H_{m0} is 0.99, and the bias is less than 0.04 m for the evaluated periods.

The Tideland buoy with MOTUS wave sensor shows good agreement with Waverider also for wave direction measurements. The mean direction has a bias of 1.4 degrees, and correlation coefficient of 0.97 integrated over the full spectrum. For energy and frequency bins between 0.05 and 0.45 Hz, the bias of mean direction from MOTUS on Tideland versus Waverider is below 5 degrees, and somewhat higher beyond this range. The RMSE values are less than 20 degrees for low frequencies (0.05–0.1 Hz) and wave energy above 10^{-3} m^2 (per 0.01 frequency bin). The wave direction measurements from one of the MOTUS sensors onboard EMM shows larger deviation from the Waverider measurements. This can be attributed to the mechanical structure of the EMM buoy disturbing the magnetic field in the area where the MOTUS sensor is mounted. When comparing the measurements including external compass, the results for wave direction from EMM are comparable to those of MOTUS onboard Tideland.

The comparisons of wave height, mean direction, and directional spread all show significantly larger differences for low (< 0.05 Hz) and high (> 0.35–0.4 Hz) frequencies. For these frequencies the wave energy is negligible. For high frequencies, the differences could have implications for remote sensing applications.

Comparisons of the wave measurements with the reference measurements (Waverider) in periods of stronger currents (> 60–80 cm/s) were limited due to missing Waverider data during such strong currents. Wave direction measurements for the MOTUS sensors onboard Tideland and EMM showed rapid variations for periods of strong currents (> 80 cm/s). By combining current and wave measurements from the same navigational buoy, the wave direction measurements could be flagged when the current exceeded a certain value. Effects of extra weight on platform buoys and different mooring lines were also investigated during the survey. Effects were seen to be small (shown in the supplementary material). This study presents data sampled with unchanged mooring lines and weights for each separate buoy.

Ardhuin et al. (2019) summarizes the accuracy levels of directional wave measurements from among others the World Meteorological Organization (WMO, 2018; Belward, 2016): Significant wave height should have measurement uncertainty of maximum 10 cm or 5% (regional, global and coastal). Mean wave direction measurements should have uncertainty of maximum 10 degrees. The accuracy limits are for a 95% confidence level (corresponding to two standard deviations) and apply to both satellite and in situ measurements of ocean wave parameters. The specified accuracy of the MOTUS wave sensor is maximum 5 cm or 1% of reading for wave height (95% confidence level), and maximum 2 degrees for wave direction (RMS 5–60 min.) (Aanderaa, 2020). There will be an additional uncertainty for the MOTUS wave measurements when the sensors are mounted on navigational buoys, which is evaluated in this study by comparing with Waverider from Datawell. As listed above, the wave height bias values were less than 4 cm for the full frequency spectrum and less than 5% for the main part of the wave spectrum when comparing at frequency and energy bins. Equivalent numbers for wave direction comparison were 1.4 degrees (Tideland) and 3 degrees (EMM) for the full frequency spectrum and less than 5 degrees for the main part of the frequency/energy bin comparisons. If this bias is added directly to the measurement uncertainty (considered to be a conservative approach), the wave height measurements of MOTUS on Tideland and EMM have an uncertainty lower than 10 cm. MOTUS on Tideland has wave directional uncertainty less than 10 degrees with good margins. For MOTUS on EMM, with external compass enabled the wave direction measurements are also less than 10 degrees.

The correlation between the measurements based on MOTUS and Waverider, is higher than 0.99 and the bias is very low. The scatter (RMSE) is equal to or lower than the scatter due to 1 h time difference (Waverider-Waverider) and may partly be due to the slightly different positions of the buoys. However, the scatter is within expected sampling variability in nearly homogeneous wave conditions. There are no significant systematic deviations between the buoys. Within the wave range of the validation period which involved several storms with H_{m0} up to 10 m, the MOTUS sensors mounted in any of the positions on the two buoys seem to be working as good or better than the Waverider, considering Waverider's problems during times with strong currents. Verification of wave models from either hindcast or forecast usually show a correlation of around 0.9–0.98, see e.g. Reistad et al. (2011), and thus MOTUS wave sensor data can be used to improve the wave models through verification.

5. Conclusions

The study presented here shows that a cost-effective micro-electro-mechanical sensor system (MOTUS, Aanderaa Data Instruments) installed on navigational or coastal buoys, provides good measurements of wave height and wave direction. The wave measurements are validated against measurements from a Waverider buoy from Datawell, which is a designated wave measurement buoy. Wave data used in the present validation cover the period 6th December 2017 to 21st March 2018, during which there were four storms with wave heights (H_{m0}) reaching 6 m and more. For equivalent wave height measurements per frequency bin (0.01 Hz) above 0.05 Hz, the MOTUS wave sensor had less than 7% and 10% bias when mounted on a Tideland navigational buoy and an EMM coastal buoy, respectively, compared to the Waverider. However, biases were mostly within ±3%. The correlation coefficient for the wave height over the full frequency spectrum (0.03–0.5 Hz) was 0.99, and the bias compared to Waverider was 0.04 m. Wave direction measurements for the Tideland navigational buoy show a bias of 1.4 degrees and a correlation coefficient of 0.97 for the full frequency spectrum. For wave direction at frequencies between 0.05 and 0.45 Hz, the MOTUS wave sensor had less than 5 degrees bias compared to Waverider. For the EMM coastal buoy, there was magnetic interference affecting the directional measurements. With a correction based on an external compass correction, the wave directional measurements had negative bias values of less than 10 degrees compared to Waverider. This leads to the conclusion that a MOTUS wave sensor onboard navigational or coastal buoys provides in situ directional wave measurements with measurement uncertainties well within the recommended accuracy levels.

CRediT authorship contribution statement

Camilla Saetre: Investigation, Writing – original draft, Visualization, Formal analysis. **Harald Tholo:** Software, Writing – review & editing, Visualization, Data curation, Conceptualization. **Jostein Hovdenes:** Writing – review & editing, Visualization, Conceptualization, Project administration. **Jan Kocbach:** Investigation, Writing – review & editing, Visualization, Formal analysis. **Anne Ansnes Hageberg:** Conceptualization, Project administration. **Inge Klepsvik:** Conceptualization, Data curation. **Ole Johan Aarnes:** Writing – review & editing, Visualization, Validation. **Birgitte Rugaard Furevik:** Writing – review & editing, Visualization, Validation. **Anne Karin Magnusson:** Writing – review & editing, Validation.

Declaration of competing interest

The authors declare the following financial interests/personal relationships which may be considered as potential competing interests: The following authors have no known competing financial interests or personal relationships that could have appeared to influence the work reported in this paper: Camilla Sætre, Jan Kocbach, Anne Ansnes Hageberg, Inge Klepsvik, Ole Johan Aarnes, Birgitte Rugaard Furevik and Anne Karin Magnusson.

The following authors are employed in Aanderaa Data Instruments AS, a Xylem brand, producing the wave sensors (MOTUS) validated in the study: Harald Tholo and Jostein Hovdenes. The navigational buoys used in the project are supplied from Tideland, a Xylem brand, and from Xylem Analytics.

This work was part of the research project Flexible and cost-effective wave sensor, coordinated by Aanderaa Data Instruments AS, funded by the Research Council of Norway (project no. 256521). The data analysis was performed by authors employed at the University of Bergen and NORCE Norwegian Research Centre. Discussions of results and writing of the manuscript paper were done in collaboration with all listed authors.

Data availability

Data will be made available on request.

Appendix A. Supplementary material

Supplementary material related to this article can be found online at https://doi.org/10.1016/j.oceaneng.2022.113161.

References

Aanderaa, 2020. Data and spesification sheet: MOTUS wave sensor 5729. https://www.aanderaa.com/productsdetail.php?MOTUS-Tideland-SB-138P-56.

Abdalla, S., Dinardo, S., Benveniste, J., Janssen, P.A., 2018. Assessment of CryoSat-2 SAR mode wind and wave data. Adv. Space Res. (ISSN: 0273-1177) 62 (6), 1421–1433.

Alliance for Coastal Technologies, 2007. Observations of directional waves, wave sensor technologies. http://aquaticcommons.org/3108/1/ACT_WR07-03_Wave_Sensor.pdf.

Ardhuin, F., Stopa, J.E., Chapron, B., Collard, F., Husson, R., Jensen, R.E., Johannessen, J., Mouche, A., Passaro, M., Quartly, G.D., Swail, V., Young, I., 2019. Observing sea states. Front. Mar. Sci. (ISSN: 2296-7745) 6, 124. http://dx.doi.org/10.3389/fmars.2019.00124, URL https://www.frontiersin.org/article/10.3389/fmars.2019.00124.

Belward, A., 2016. The Global Observing System for Climate: Implementation Needs. Technical Report GCOS-200, World Meteorological Organization.

Cavaleri, L., Abdalla, S., Benetazzo, A., Bertotti, L., Bidlot, J.-R., Breivik, O., Carniel, S., Jensen, R., Portilla-Yandun, J., Rogers, W., Roland, A., Sanchez-Arcilla, A., Smith, J., Staneva, J., Toledo, Y., van Vledder, G., van der Westhuysen, A., 2018. Wave modelling in coastal and inner seas. Prog. Oceanogr. (ISSN: 0079-6611) 167, 164–233.

Christakos, K., Björkqvist, J.-V., Tuomi, L., Furevik, B.R., Breivik, Ø., 2021. Modelling wave growth in narrow fetch geometries: The white-capping and wind input formulations. Ocean Model. (Oxford) (ISSN: 1463-5003) 157.

Christakos, K., Furevik, B.R., Aarnes, O.J., Breivik, O., Tuomi, L., Byrkjedal, O., 2020. The importance of wind forcing in fjord wave modelling. Ocean Dyn. (ISSN: 1616-7341) 70 (1), 57–75.

Datawell BV, 2020. Datawell waverider reference manual DWR-MKIII, DWR-g, WR-sg. https://www.datawell.nl/Support/Documentation/manuals.aspx.

Furevik, B.R., Agustsson, H., Borg, A.L., Midjiyawa, Z., Nyhammer, F., Gausen, M., 2020. Meteorological observations in tall masts for the mapping of atmospheric flow in norwegian fjords. Earth Syst. Sci. Data (ISSN: 1866-3516) 12 (4), 3621–3640. http://dx.doi.org/10.5194/essd-12-3621-2020.

Furevik, B.R., Lønseth, L., Borg, A.L., Neshaug, V., Gausen, M., 2016. URL http://dx.doi.org/10.21343/ef2d-jp97 Oceanographic observations for the Coastal Highway E39 project in Mid-Norway,

Herbers, T.H.C., Jessen, P.F., Janssen, T.T., Colbert, D.B., MacMahan, J.H., 2012. Observing ocean surface waves with GPS-tracked buoys. J. Atmos. Ocean. Technol. 29 (7), 944–959. http://dx.doi.org/10.1175/JTECH-D-11-00128.1, URL https://journals.ametsoc.org/view/journals/atot/29/7/jtech-d-11-00128_1.xml.

Jensen, R., Swail, V., Bouchard, R., 2021. Quantifying wave measurement differences in historical and present wave buoy systems. 71, pp. 731–755. http://dx.doi.org/10.1007/s10236-021-01461-0.

Jensen, R., Swail, V., Lee, B., OReilly, W., 2011. Wave measurement evaluation and testing. In: Proc. of the 12th International Workshop on Wave Hindcasting and Forecasting.

Krogstad, H.E., Wolf, J., Thompson, S.P., Wyatt, L.R., 1999. Methods for intercomparison of wave measurements. Coast. Eng. (Amsterdam) (ISSN: 0378-3839) 37 (3), 235–257.

Kuik, A.J., van Vledder, G.P., Holthuijsen, L.H., 1988. A method for the routine analysis of pitch-and-roll buoy wave data. J. Phys. Oceanogr. 18 (7), 1020–1034. http://dx.doi.org/10.1175/1520-0485(1988)018<1020:AMFTRA>2.0.CO;2, URL https://journals.ametsoc.org/view/journals/phoc/18/7/1520-0485_1988_018_1020_amftra_2_0_co_2.xml.

Liu, Q., Lewis, T., Zhang, Y., Sheng, W., 2015. Performance assessment of wave measurements of wave buoys. Int. J. Mar. Energy (ISSN: 2214-1669) 12, 63–76.

Liu, Y., Wang, X., You, J., Chen, C., 2020. Ocean wave buoy based on parallel six-dimensional accelerometer. IEEE Access 8, 29627–29638. http://dx.doi.org/10.1109/ACCESS.2020.2971711.

Longuet-Higgins, M.S., Cartwright, D.E., Smith, N.D., 1965. Observations of the directional spectrum of sea waves using the motions of a floating buoy. In: Ocean wave spectra, proc. Conf., Easton, Md., May 1–4, 1961, Prentice-hall, N.J., 111–132. Deep-Sea Res. Oceanogr. Abstracts.

Luther, L., Meadows, G., Buckley, E., Gilbert, S., Purcell, H., Tamburri, M., 2013. Verification of wave measurement systems. http://dx.doi.org/10.4031/MTSJ.47.5.11.

OReilly, W., Herbers, T., Seymour, R., Guza, R., 1996. A comparison of directional buoy and fixed platform measurements of Pacific swell. J. Atmos. Ocean. Technol. (ISSN: 0739-0572) 13 (1), 231–238.

Reistad, M., Breivik, Ø., Haakenstad, H., Aarnes, O.J., Furevik, B.R., Bidlot, J.-R., 2011. A high-resolution hindcast of wind and waves for the north sea, the norwegian sea, and the barents sea. Reistad, M., Breivik, H. Haakenstad, O. J. Aarnes, B. R. Furevik, and J.-R. Bidlot (2011) A high-resolution hindcast of wind and waves for the North Sea, the Norwegian Sea, and the Barents Sea, J. Geophys. Res., 116, C05019, doi:10.1029/2010JC006402. J. Geophys. Res.: Oceans (ISSN: 0148-0227) 116 (C5), n/a.

Tengberg, A., Weiss, G., Roach, D., 2018. Directional wave, currents and environmental monitoring from navigation and hydrography buoys: An introduction to motus. In: 2018 OCEANS - MTS/IEEE Kobe Techno-Oceans. OTO, pp. 1–10. http://dx.doi.org/10.1109/OCEANSKOBE.2018.8559239.

Tideland, a Xylem brand, 2022. SB-138P sentinel® buoy. http://tideland-tideland-stage-1088501270.us-east-1.elb.amazonaws.com/products/buoys/sb-138p, (Accessed 04 June 2022).

WMO, 2018. Guide to instruments and methods of observation: Volume I - Measurement of meteorological variables. WMO-no. 8. https://library.wmo.int/index.php?id=12407&lvl=notice_display#.YcG_3lko_b1.

Xylem Analytics, 2022. YSI emm2.0 coastal buoy. https://www.xylemanalytics.co.uk/ysi-emm2.0-coastal-buoy/. (Accessed 04 June 2022).